THESIS

CAPTURING THE ONSET OF SNOWMELT IN HIGH ELEVATION POST-FIRE LANDSCAPES

Submitted by

Marin MacDonald

Department of Ecosystem Science and Sustainability

In partial fulfillment of the requirements
For the Degree of Master of Science
Colorado State University
Fort Collins, Colorado
Summer 2026

Master's Committee:

Advisor: Steven R. Fassnacht

Daniel McGrath

Molly Tedesche

ABSTRACT

CAPTURING THE ONSET OF SNOWMELT IN HIGH ELEVATION POST-FIRE LANDSCAPES

In the Western United States, the increased threat of fire has impacted ecosystem health in high-elevation areas, as well as the associated water resources. Although fires have historically occurred in low-elevation forests adapted to fire conditions, in recent years, Colorado has experienced several high severity fires at higher elevations in areas critical to water storage. With much of the west relying on snow-dominated watersheds for water storage and availability, assessing the impacts of these fires on snowpack is critical.

Although there has been recent research assessing snowpack trends in Colorado, remote sensing techniques using Sentinel-1 (S1) have had limited application. This study uses S1 Synthetic Aperture Radar (SAR) to detect the onset of snowmelt in high severity, high elevation sites in the Southern Rocky Mountains of Colorado and Southern Wyoming. Sites were compared to assess the interannual variability of the onset of snowmelt post-fire, and a multivariate regression was used to determine the effect of northness and elevation on the onset melt dates. Results were compared to SNOTEL station closest to each fire for comparing onset of melt dates in relation to peak SWE.

TABLE OF CONTENTS

ABSTRACT ii

Chapter 1 - Introduction 1

Chapter 2 - Literature Review 5

Wildfires and Snow 5

Remote Sensing Techniques and Snow 7

Chapter 3 - Study Area 12

Chapter 4 - Data Access 20

Sentinel-1 Data 20

In-Situ Data 21

Terrain Data 21

Burn Severity Data 21

Chapter 5 – Methodology 29

Sentinel-1 Processing 29

Sentinel-1 Analysis 30

SNOTEL Comparison 33

Chapter 6 - Results 34

Yearly Onset of Mel Distribution and Variability 34

Melt Distribution 34

Interannual Onset of Melt Variability 36

Topographic Controls on the Onset of Melt 38

Elevation 38

Northness 39

Diurnal Anisotropic Heating 40

Multivariate Regression Analysis 41

Spatial Autocorrelation and Clustering 42
SNOTEL Comparison 44
Chapter 7 – Discussion and Conclusion 47
Onset Melt Distribution and Interannual Variability 47
Impact of Topographic and Geographic Controls 48
Local Timing Patterns 50
SNOTEL Comparison 51
Future Work 52
Conclusion 53
APPENDIX 55
REFERENCES 64

1. INTRODUCTION

Across the Western United States, snow dominated watersheds provide essential water resources (Barnett et al., 2005; Bales et al., 2006). These montane watersheds store critical water sources in the form of snow, which influences water availability in the spring during snowmelt (Mote et al., 2005; Stewart et al., 2005; Li et al., 2017; Koshkin et al., 2022; Hale at al., 2023). Water from snowmelt that flows downstream is especially important during the dry summer months when inputs from precipitation are more variable and demand from ecosystems, people, agriculture, and evaporative losses are highest (Bales et al., 2006; Dozier, 2011; Mankin et al., 2015; Mote et al., 2018; Immerzeel et al., 2019; Elias et al., 2021). In areas like Colorado's Front Range, and other urban areas of the Western United States, population increases have put further strain on these montane watersheds (McDonald et al., 2011; Warziniack & Brown, 2019; Heidari et al., 2021; Warziniack et al., 2024).

Assessing how much water is available during prolonged dry months requires an understanding of snow accumulation, runoff efficiency, and timing, all of which are facing impacts due to climate change (Cayan, 1996; Mote, 2003; Barnett et al., 2005, Hamlet et al., 2005; Regonda et al., 2005; Pierce et al., 2008; McCabe & Wolock, 2009; Hammond et al., 2018; Fassnacht et al., 2018; Fassnacht et al., 2020).With declines in peak snow water equivalent (SWE) and earlier onset of snowmelt in recent years (Dudley et al., 2017; Elias et al., 2021; Hale et al., 2023), it is becoming increasingly important to study how these dynamics are changing (Stewart et al., 2008; Fassnacht et al., 2018)

Climate change is also increasing the occurrence of high elevation wildfires across the West, creating new post-fire landscapes, leading to changes in forest structure and snow retention in these areas (Higuera et al., 2021; Kampf et al., 2022; Wasserman & Mueller, 2023). Historically, fires in Colorado have been mainly in low elevation Ponderosa Pine forests, adapted to frequent low severity fires during the summer months (Kaufmann et al., 2000; Veblen et al., 2000; Baker, 2018; Battaglia et al., 2018; Hagmann et al., 2021; Parks et al., 2023). Ponderosa forest fires have a recurrence of five to twenty-five years while forest communities at higher elevation have historically had a fire recurrence of 50-300 years, depending on the forest structure (Table 1.1) (Colorado State Forest Service, 2023). However, as drought conditions have become more frequent, fires have spread to higher elevation forests and are burning at higher severity over larger areas at a recurrence of less than 50 years (Stevens-Rumann et al., 2017; Alizadeh et al., 2021; Busby et al., 2020; Kampf et al., 2022; Davis et al., 2023). These forests can take hundreds of years to regenerate, leaving large areas of the mountains without canopy cover, an essential piece of snow energy dynamics (Mazzotti et al., 2022; Sun et al., 2022; Rutter et al., 2023).

Table 1.1 Tree types and fire recurrence in Colorado

Tree Type	**Fire recurrence**
Ponderosa Pine	5-25 years (Colorado State Forest Service)
Lodgepole Pine	100-300 years (Turner et al., 2019)
Engleman Spruce	150-300+ years (Colorado State Forest Service, 2025)
Sub-alpine Fir	150-300+ years (Colorado State Forest Service, 2025)
Mixed Spruce-Fir	300+ years (Colorado State Forest Service, 2025)

Summer and fall of 2020 brought an unprecedented fire season for Colorado, with five high severity wildfires across the forests of the state (Kampf et al., 2022). The Cameron Peak fire, the largest in Colorado history, spanned roughly 208,000 acres, and burned in high elevation forests which store snowpack (McGrath et al., 2023). Fires have devastating consequences on watershed health, impacting water retention in soils and water quality of runoff and rivers (Thompson et al., 2013). Previous studies have found changes in snow disappearance date (SDD) and snow duration in high elevation burn areas, specifically areas with more sun exposure (Kampf et al., 2022; Reis et al., 2024). Burned areas also have shown to have reduced maximum snow water equivalent (SWE) values, and earlier maximum SWE dates (Giovando & Niemann, 2022). These impacts, combined with the expected decrease in snowpack in the Western United States (Evan, 2019; Livneh & Badger, 2020), has led to an even greater need to understand the spatio-temporal and interannual variability of snowmelt (Clow, 2010) in these areas.

With snow being a critical source of water storage, the Natural Resources Conservation Service (NRCS) created a network of snow telemetry (SNOTEL) sites designed to estimate runoff volumes from snow throughout the Western United States (USDA, 2025). Although these sites have a long period of record, they only provide point source data, and do not cover the spatial variability of snowpack (Daly et al., 2000; Meromy et al., 2013). When considering the challenge of surveying in montane terrain, remote sensing techniques, such as satellite data, provide a way to analyze larger study areas for snowpack properties at a regular frequency.

The European Space Agency's (ESA) Sentinel missions, the constellation satellites Sentinel-1A and 1B (S1) provide applications in snow and water resources through synthetic aperture radar (SAR) (ESA, 2024). With a return interval of 5-8 days at mid-latitude depending on constellation availability, these satellites do not have as fine of a temporal resolution as a

SNOTEL site. However, the spatial resolution allows for the monitoring of larger study sites on a consistent schedule during the winter and spring months. Radar remote sensing, such as from Sentinel-1's C-band SAR, has proven useful in detecting changes in snowpack, such as the onset of melt, due to the sensitivity of microwave radiation (Marin et al., 2020). With SAR, liquid water can absorb the received signal, meaning the returned backscatter signal is very weak and can be differentiated from dry surface conditions, a very useful property for determining when versus dry snow conditions (Nagler et al., 2016; Gagliano et al., 2023).

With changes in snow timing and properties, a combination of SNOTEL measurements and satellite data provides a way to increase understanding of the spatio-temporal variability of snow at a larger scale and more cost-effective price-point than paid services like Airborne Snow Observatories flights. This study aimed to assess the viability of using Sentinel-1 C-band SAR to determine the onset of snowmelt using the minimum backscatter date method (Marin et al., 2020, Gagliano et al., 2023) within 5 mid-latitude post-fire landscapes in the Southern Rocky Mountains. The research objectives of this project focused on: 1) using Sentinel-1 to determine the onset of snowmelt date for high severity post-fire pixels, 2) assess the interannual variability in the onset of snowmelt for high severity pixels, 3) determine the relationship between the onset of snowmelt and topographic features of the study areas, and 4) compare the onset of snowmelt to SNOTEL peak snow water equivalent (SWE) values for the period of record (2021-2025).

2. LITERATURE REVIEW

2.1 Wildfires and Snow

With the potential for largescale wildfire activity in the Western United States growing (Barbero et al., 2015; Keyser et al., 2017), the impacts which these events have on snowpack have been increasingly studied. Historically, wildfires in Colorado occurred in low elevation Ponderosa Pine forests with 30 to 40-year recurrence interval and variable severity regime (Sherrif & Veblen, 2007). Higher severity fires were found to have a recurrence of roughly 400 years (Williams & Baker 2012). However, the occurrence of large-scale high severity fires has been increasing (Marlon et al., 2012). This is due to several factors, including changes in climate, forest management, and increased human interactions. In the 20th century, the fire regime was mainly controlled by climate (Littel et al., 2009). In a study conducted by Marlon et al. (2012), charcoal and fire-scar data were compared to historical fire data, and concluded that due to suppression and changing climate, there has been an increase in "fire deficit", leading to a greater frequency of fires in a shorter time span. During the 20th century, suppression of wildfire led to a buildup in fuels (Agee & Skinner, 2005; Kreider et al., 2024). In addition, longer dry periods have increased the risk of fire as well, causing greater amounts of fuel loading and severe fire conditions (Gedalof et al., 2005; Westerling et al., 2006; Morgan et al., 2008; Westerling, 2016; Keyser et al., 2017). Topography, especially aspect, slope, and elevation, can also impact fire growth and severity (Dillon et al., 2011; Kane et al., 2015; Estes et al., 2017; Povak et al., 2018). Ultimately, this increase in frequency of high elevation fires at larger scale and severity is unprecedented considering the history of the fire regime in Colorado (Kampf et al., 2022).

In addition to landscape change, recent wildfires in montane watersheds pose threats to watershed health (Bladon et al., 2014; Hallema et al., 2018; Rhoades et al., 2018; Hohner et al., 2019; Robinne et al., 2019; Robinne et al., 2021; Kampf et al., 2022). Researchers have also found that a fire's intensity and duration, and its location in a watershed, can determine the severity of impacts (Ice et al., 2004). Since fires cause watershed impacts, as fires have more frequent occurrence in high elevation areas, snowpack is affected too. When forested watersheds burn at high severity, there is a large loss in canopy, which often acts as a form of interception of snow during the winter season (Reis et al., 2024). In turn, this allows more snow to accumulate (Winkler, 2011). However, this loss of canopy coverage can lead to other issues. In the years post fire, debris and ash from burned trees can lead to decreased snow albedo, which affects the amount of shortwave radiation that is absorbed by the snowpack (Gleason et al., 2013; Gleason & Nolin, 2016; Kampf et al., 2022; Reis et al., 2024; Surunis & Gleason, 2024). With increased shortwave radiation from direct sunlight and decreased longwave radiation due to lack of canopy cover, there is an imbalance. Lack of tree cover can also lead to more wind redistribution (Ewing and Fassnacht, 2007; Burles & Boon, 2011), as open spaces can create potential for more snow movement, leading to greater shifts in sensible and latent heat fluxes. Due to the spatial variability of snow, wildfire impacts on snow distribution and melt vary depending on terrain, climate, and vegetation (Harpold et al., 2013; Lundquist et al., 2013; Maxwell et al., 2018; Kampf et al., 2022).

In the Western United States, the amount of montane area affected by fires is increasing (Kampf et al., 2022). With more fires occurring within seasonal snow zones, there may be decreases in SWE, and earlier maximum peak SWE (Giovando & Neimann, 2022). Following the Cameron Peak Fire, Kampf et al. (2022) compared burned and unburned sites at varying snow zones to assess changes in peak SWE and snow depth. They found that in 2021, the year immediately following the fire, burned sites had earlier peak SWE dates, and generally lower SWE throughout the season at sites where melt generally began between late April and early May. This indicates earlier snow loss post-fire in areas of seasonal snow, which could have long term impacts on water storage and availability in these areas.

2.2 Microwave Remote Sensing and Snow

Microwave remote sensing has been used for more than 50 years (e.g., Foster et al., 1984; Chang et al., 1987) to analyze SWE for shallow snowpacks. While in-situ measurements can provide insights into the properties of a snowpack in the area which they are collected, the high spatial variability of snow means these measurements are often not representative of an area as a whole (Meromy et al., 2013; Gascoin et al., 2019). Because of this, the implementation of microwave remote sensing allows for the assessment of snowpack over a larger scale, helping to better account for the spatial variability of snow presence and snowpack properties, especially in montane regions (Foster et al., 2004; Li et al., 2012). Further, unlike optical remote sensing, microwave remote sensing is minimally impacted by cloud cover.

Starting with the launch of the Scanning Multichannel Microwave Radiometer (SMMR), passive microwave has been assessed as a method for detecting snow properties at watershed scale in shallow, non-wet snowpacks (Rango & Litten, 1976, Hall et al., 2006). Since the late 20th century, it has been understood that spaceborne passive microwave has the potential to help in determining snow water equivalent (SWE) and the onset of snowmelt with the help of post-processing algorithms (Chang et al., 1979; Foster et al., 1984; Dietz et al., 2012; Frei et al., 2012). Early studies proved the viability of this methodology through comparison with in-situ ground measurements (Hall et al., 1991; Derksen et al., 2005; Cordisco et al., 2006; Kongoli et al., 2007) and determined the limitations of passive microwave, such as vegetative cover and montane terrain decreasing the accuracy of returned images (Walker & Goodison, 1993; Tait, 1998).

With increasing availability of spaceborne satellite options, optical imagery has also been a widely used method in the snow community. The three main sensors used in this methodology are the National Aeronautics and Space Administration's (NASA) Moderate Resolution Imaging Spectroradiometer (MODIS) satellite, the United States Geological Survey's (USGS) Landsat satellite, and the European Space Agency's (ESA) Sentinel-2 constellation (Justice et al., 1998; Drusch et al., 2011; Roy et al., 2014). All three of these satellites provide the bands needed to calculate metrics such as Normalized Difference Snow Index (NDSI). MODIS provides daily returns at 500m resolution (Hall et al., 1995), Landsat-8 provides a return every 16 days at 30m resolution, and Sentinel-2 provides a 20m resolution with a variable return depending on location (Gascoin et al., 2019; Revuelto et al., 2021). Since Sentinel-2 was launched in 2015 (ESA, 2024), it has a shorter available period of record than Landsat and MODIS but provides a finer scale image at a faster rate of return (Hofmeister et al., 2022). Previous studies have used coarse MODIS data to complete large scale data analysis of Snow Covered Area (SCA) and fractional snow cover (fSCA) to produce snow maps (Hall et al., 2002; Painter et al., 2009; Moore et al., 2015; Saavedra et al., 2015; Mason et al., 2018; Hammond et al., 2018) and determine snow presence and persistence (Klein and Barnett, 2003; Parajka & Blöschl, 2006; Pu et al., 2007; Gafurov & Bardossy, 2009). For example, in Moore et al. (2015), MODIS data was downscaled from 500m resolution to produce SCA images across Western North American mountain ranges to define elevations for intermittent, transitional, and persistent snow zones. Landsat has been used to generate finer scale SCA maps, but due to its longer return period has greater limitations in areas with increased cloud cover (Parajka and Blöschl, 2008; Gascoin et al., 2015). To reduce resolution or temporal limitations, recent studies have combined MODIS and Landsat with Sentinel-2 imagery. In Revuelto et al. (2021), MODIS imagery was downscaled spatially using trained Sentinel-2 data. This improved the resolution and allowed for a longer record period than Sentinel-2 (Revuelto et al., 2021).

Although spectral imagery can be highly beneficial for determining SCA and other snow properties, it is limited by nightfall and cloud cover. When clouds are present, no data can be inferred from the imagery. However, Synthetic Aperture Radar (SAR), an active microwave option, offers a way to fill this gap. SAR, which transmits microwave signals, returns a backscatter value rather than a spectral image, helping in determining the physical properties of a surface (ASF, 2024). SAR is especially useful in determining the presence of liquid water on a surface and has been used as a method to determine SWE and onset of snowmelt, as it is highly sensitive to liquid water content within a snowpack (Marin et al., 2020). During snow season, when the snow is frozen, the returned signal from SAR is from surface scattering (Matzler, 1987; Shi and Dozier, 1995; Nagler and Rott, 2000). However, as it gets closer to peak SWE, and ablation begins, the main returned signal comes from the water in the snowpack, as opposed to surface scattering (Shi and Dozier, 1995; Nagler and Rott, 2000). With SAR, there is an inverse correlation between backscatter value and liquid water content (LWC) in a snowpack. This means that as LWC increases during melt season, the returned backscatter value decreases, with the lowest backscatter value of the season being the onset of melt (Marin et al., 2020). Physical snowpack properties, such as depth, density and grain size, as well as terrain features and canopy coverage of an area, can impact the magnitude of a SAR backscatter (Liu et el., 2006; Pivot, 2012; Darychuk et al., 2022).

The ESA's Sentinel-1 constellation, which is C-band SAR with a frequency of 5.405 GHZ, is the main spaceborne microwave imager currently used for snow. Sentinel-1 in Interferometric Wide swath (IW) mode, which offers dual-polarized channels (VV and VH), can be used to generate melting snow maps based on change detection for classification of dry versus wet snow (Nagler et al., 2016). Other studies have used the dual-polarization with satellite or derived azimuth angles to retrieve backscatter values for the detection of wet versus dry snow using change detection across various field sites (Li et al., 2017; Lund et al., 2020; Liu et al., 2020; Marin et al., 2020; Liang et al., 2021; Lund et al., 2022; Tedesche et al., 2022; Mahmoodzada et al., 2022; Gagliano et al., 2023). Using Sentinel-1 SAR to track melt and diurnal cycling of snow (melt-refreeze) may be beneficial in assessing snowpack energy balance, as well as used in runoff forecasting and modeling (Lund et al., 2020). Different relative orbits and incidence angles can be used to isolate ideal wet snow incidence angles and orbits for specific sites and conditions (Lund et al., 2022; Drychuk et al., 2023). Multiple available Sentinel-1 orbits (both ascending and descending), incidence angles, and polarizations ensure greater temporal resolution for mid and high latitude sites (Gagliano et al., 2023). With more polarizations and incidence angles, the method of Galiano et al. (2023) returned reliable onset of melt dates for the Mount Ranier study site consistent with in-situ measurements.

From previous work, the use of C-band SAR for determining SWE and onset of snowmelt clearly has viable applications, yet most sites studied were in polar regions, on glaciers, or in the high alpine. These areas can provide study sites where there is less variability in energy inputs and less vegetative cover than forested environments. There has been limited use of the Nagler et al. (2016) methodology in more mid-latitude snowpacks, especially in Colorado and Southern Wyoming. This could in part be due to Sentinel-1's decreased accuracy at snow retrieval under dense canopy cover (Nagler et al., 2016; Lievens et al., 2022), and a less consistent backscattering difference from a frozen or snow-free reference (Hoppinen et al., 2024). The Gagliano et al. (2023) study confirms that to use this backscatter minima methodology to define the onset of melt date, there must be less than 50% canopy coverage in a pixel. For the study conducted at Mount Rainier, areas were masked using a world landcover dataset to reduce erroneous backscatter returns.

Although Sentinel-1's sensitivity to vegetation generally makes its applications limited in areas like Colorado, high severity burn areas offer a unique opportunity to use this methodology. In high severity burn areas, where vegetative cover has been reduced, Sentinel-1's 5.405 GHZ wavelength can accurately return a backscatter value for the snow within the pixel. Therefore, the application of the Gagliano et al. (2023) Sentinel-1 derived onset of melt is viable for these high severity post-fire landscapes of Colorado and Southern Wyoming. Because of the variability of the melt season in the Southern Rockies region, increasing temporal resolution using this method is beneficial, and the multi-incidence angles and polarizations defined in Gagliano et al. (2023) was therefore used in this study. This study will offer insight into the application of this methodology in high-severity post-fire landscapes at mid-latitude and provide a more in-depth understanding of onset of melt characteristics in these areas.

3. STUDY AREA

This study focused on five high-elevation fires that occurred in Colorado and Southern Wyoming during the unprecedented fire season of 2020 (Figure 3.1, Figure 3.2). Four of these fires were in Colorado, with one predominantly located in Southern Wyoming. They ranged in size from 14,833 acres to 208,000 acres (Table 3.1). Each of these fires, unlike most previous fires, burned in higher elevation areas (Kampf et al., 2022). An average of 28% of each study area burned at MTBS differenced Normalized Burn Raio (dNBR) level 4, which has been defined as high severity. For this study, only areas in this highest burn severity were assessed, in order to align with the Sentinel-1 limited accuracy through canopy cover (Bazzi et al., 2024).

Within the five burn perimeters, severe burns occurred in both the transitional and seasonal snow zones, as defined by Richer et al. (2013). This zone is critical to seasonal water storage in Colorado, with the seasonal snow zone storing a majority of Colorados water during the winter months (Pederson et al., 2013; Fassnacht et al., 2018; Hammond et al., 2021; Hale et al., 2024). For each of these fires, the focus was high severity burn pixels in the seasonal snow zone (as defined by Richer et al., 2013; Moore et al., 2015) that retains snow throughout the winter season, every winter on record; although the transitional snow zone also holds snow for the entire winter in some years.

The study areas ranged in elevations from 1878 m to 3546 m (Table 3.1). The Cameron Peak Fire had the largest range of elevations, while Mullen had the smallest elevation range (Figure 3.3). Elevation~~s~~ across the study sites were normally distributed for all study areas, except for Mullen (Figure 3.3). The distribution of aspect values across study sites was skewed towards north-facing pixels. This is more prominently seen in the Cameron Peak and Williams Fork study areas (Figure 3.4).

In addition to the five study areas, corresponding SNOTEL stations were selected based on distance from the burn perimeters (Table 3.2). Fires were given either 2 or 3 SNOTEL stations for analysis depending on station availability and distance. Some study areas, like Williams Fork, had SNOTEL sites within 4km of the burn perimeter, while others, such as the Mullen, had stations farther away (Figure 3.5).

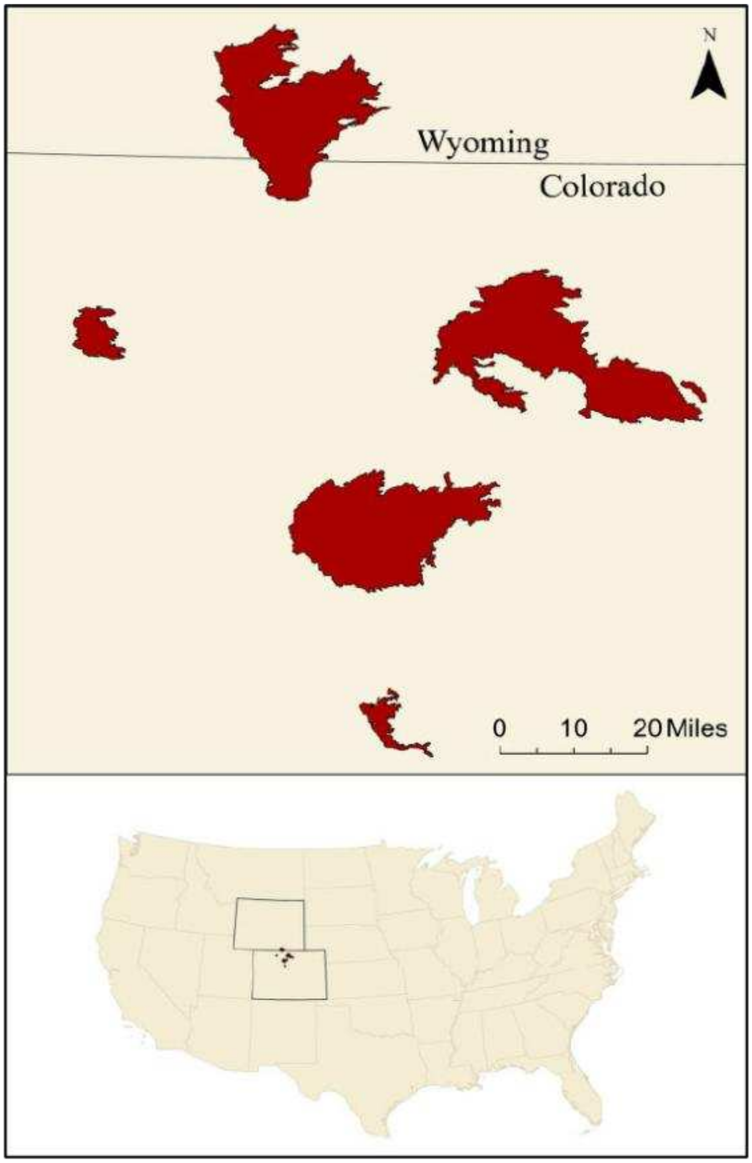

Figure 3.1 Location of the five fires within the Contiguous United States. Fire perimeters are shown in red.

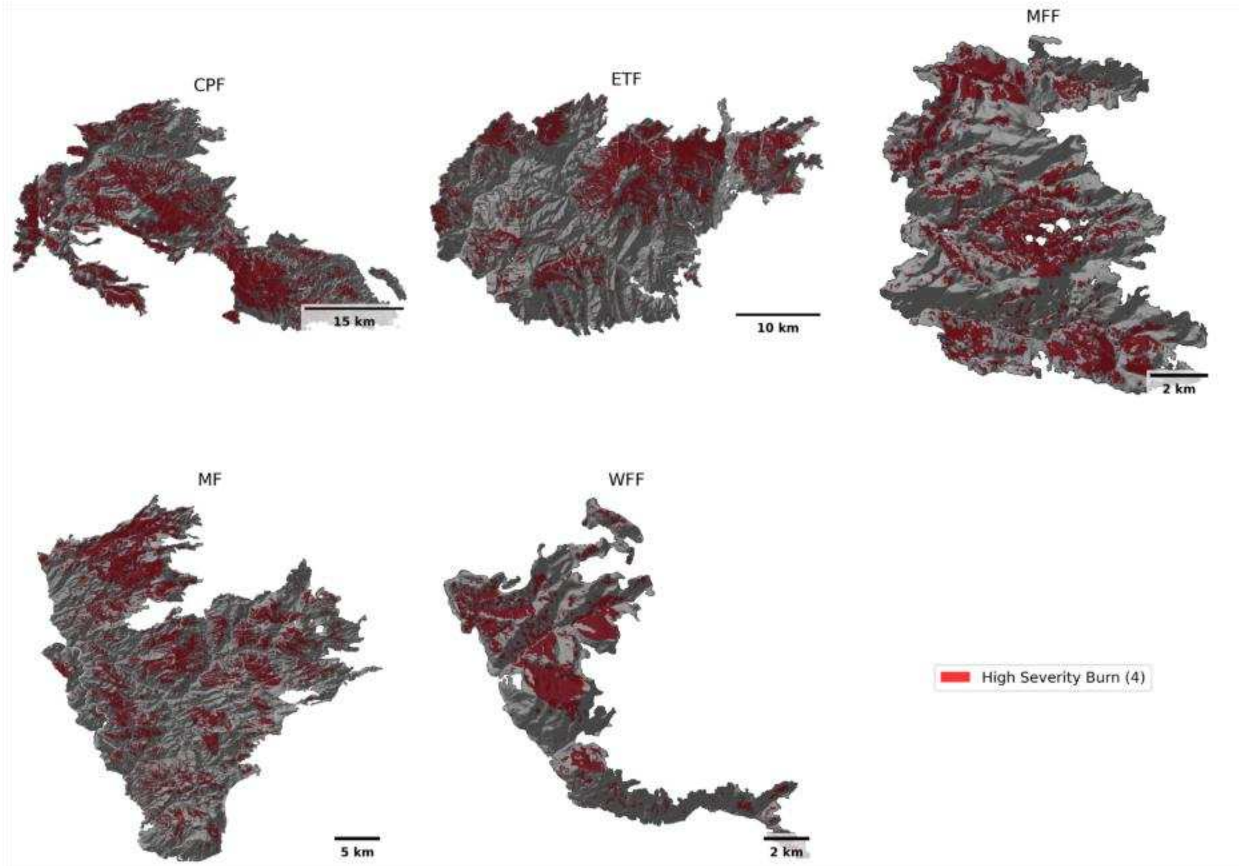

Figure 3.2 Maps of the five fire perimeters (shown in grey) with the high severity burn areas (study areas) in red.

Table 3.1 Metadata for the five study areas. Total acreage and burn severity are for the entire fire perimeters, and the elevation range and dominant aspect are for severe burn areas only. Aspect percentages indicate the percent of high severity pixels that fall into that aspect bin.

Fire	Total Area (Acres)	Severe Burn (%)	Elevation Range (m)	Dominant Aspect
Cameron Peak Fire (CPF)	208,913	38.4	1878-3523	NW (21.3%)
East Troublesome Fire (ETF)	193,812	24.9	2478-3546	NW (17.5%)
Mullen Fire (MF)	176,878	26.0	2280-3157	N (19.2%)
Middle Fork Fire (MFF)	20,433	27.3	2441-3390	N (26.2%)
Williams Fork Fire (WFF)	14,833	25.8	2642-3542	NE (28.9%)

Table 3.2 Metadata for selected SNOTEL sites. The closest fire and distance are included.

Station Name	Latitude	Longitude	Elevation (m)	Nearest Fire	Distance to Fire (km)
Long Draw Reservoir	40.51	-105.77	3045	CPF	18.35
Never Summer	40.4	-105.96	3139	ETF	19.18
Zirkel	40.79	-106.6	2841	MFF	22.66
Middle Fork Camp	39.8	-106.03	2731	WFF	4.14
Jones Pass	39.76	-105.91	3176	WFF	11.92
Cinnabar Park	41.24	-106.23	2947	MF	15.81
Lost Dog	40.82	-106.75	2847	MFF	20.96
Stillwater Creek	40.23	-105.92	2670	ETF	9.62
Phantom Valley	40.4	-105.85	2752	ETF	23.90
Roach	40.87	-106.05	2960	MF	32.58
Deadman Hill	40.81	-105.77	3121	CPF	27.02
Joe Wright	40.53	-105.89	3091	CPF	26.45
Tower	40.54	-106.68	3234	MFF	12.72
North French Creek	41.33	-106.38	3094	MF	26.46

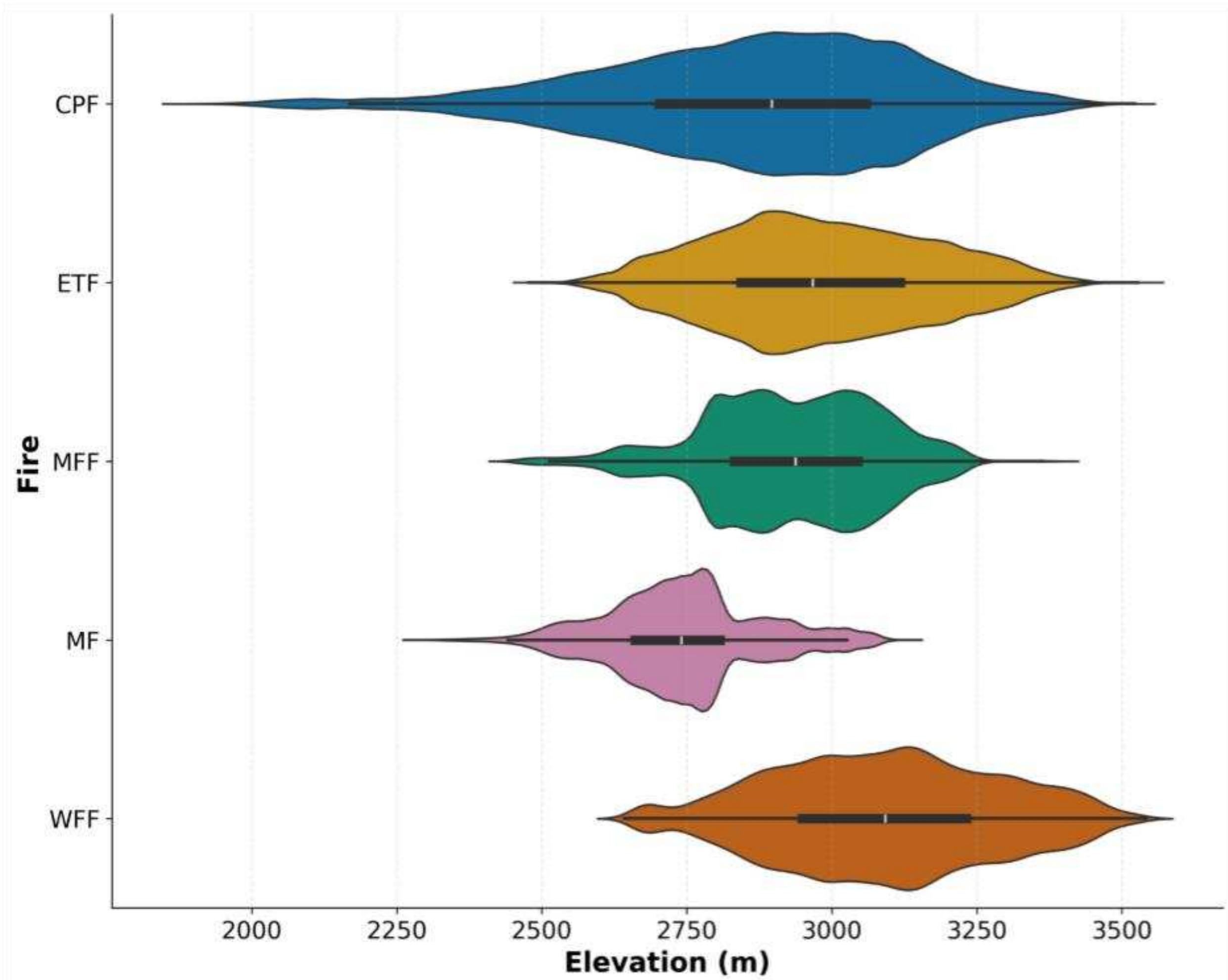

Figure 3.3 The range of elevation values for high severity pixels for all study areas. Most pixels fall into the 2750-3250 m range. Cameron Peak has a noticeably wider range of elevations.

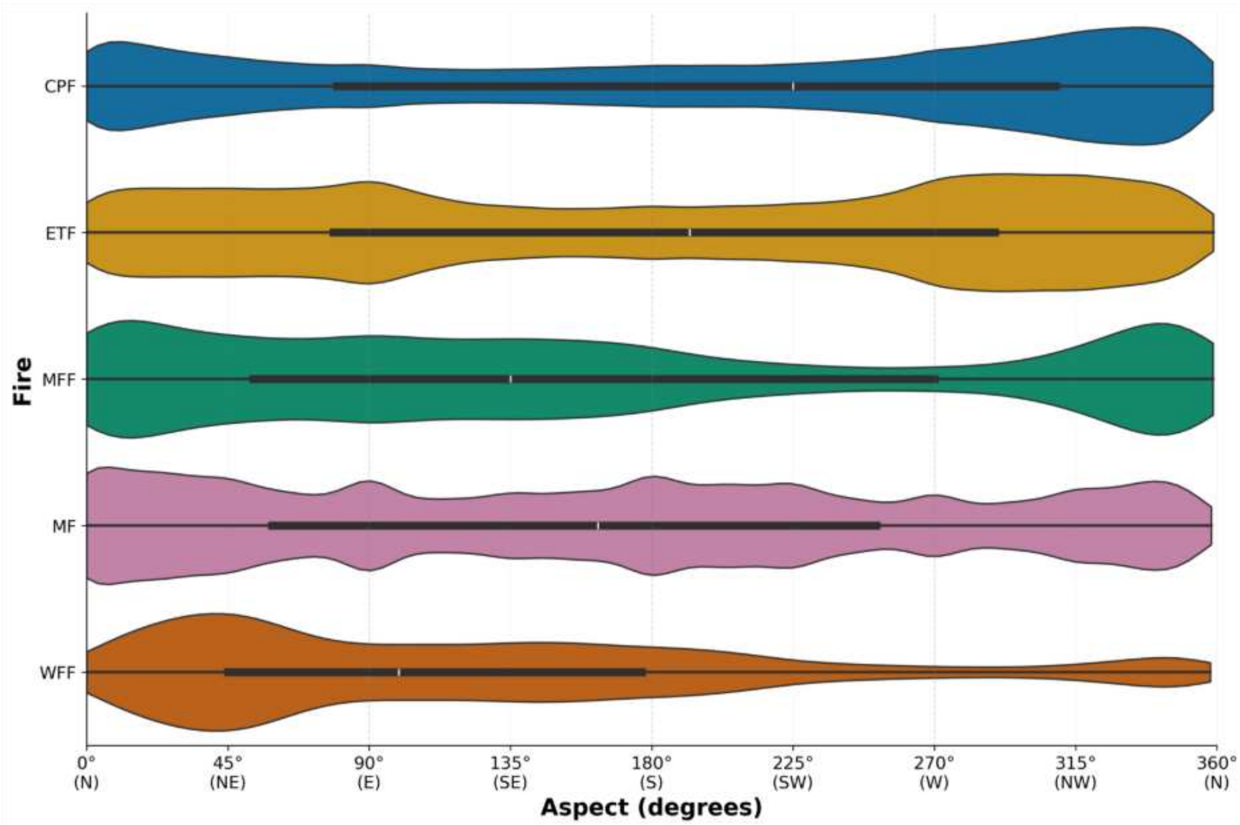

Figure 3.4 Distribution of aspect by pixel for all study sites. There is a greater concentration of north-facing pixels for all fires.

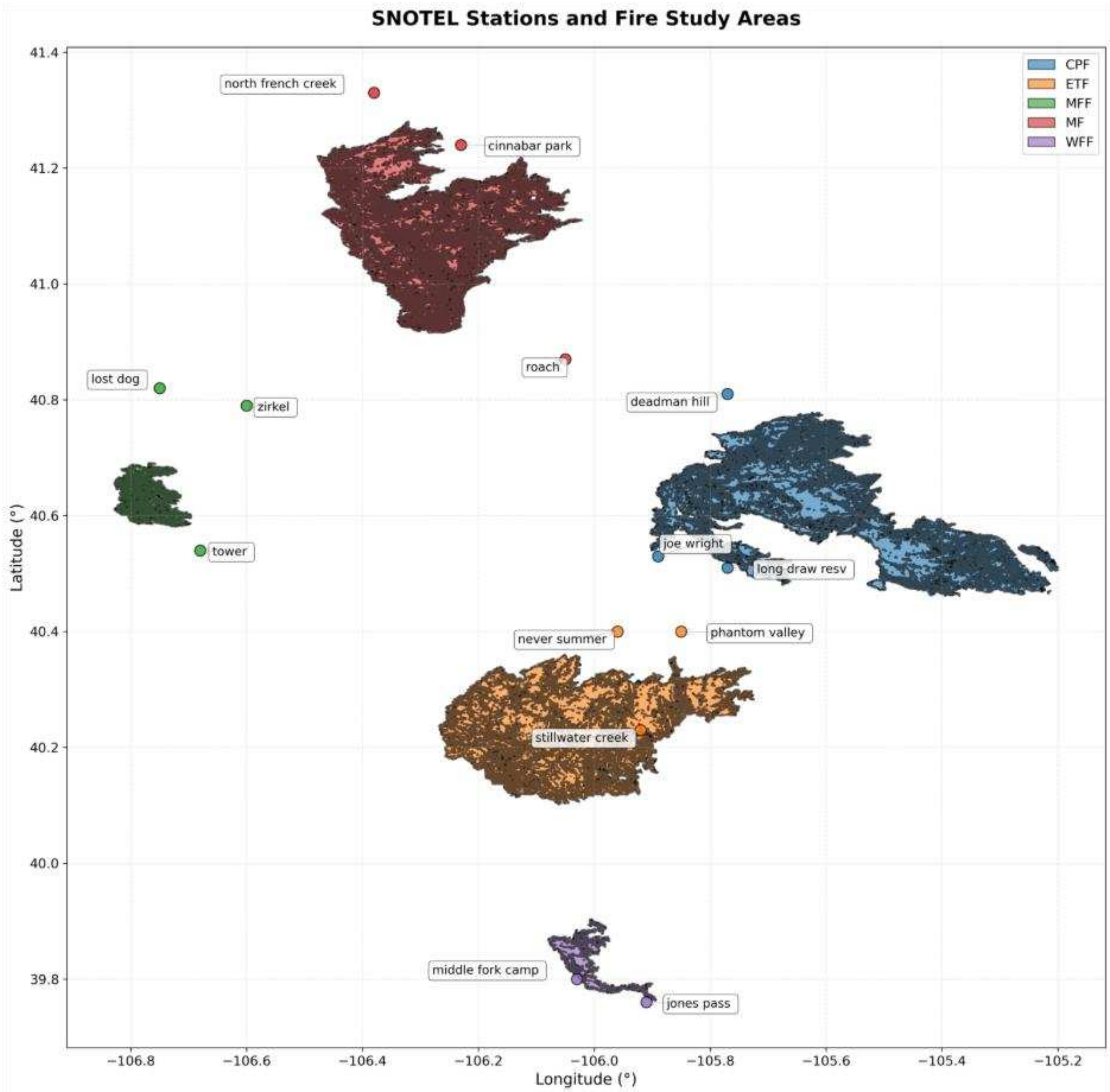

Figure 3.5 Map of the five fires and nearby SNOTEL stations. Stations are color coded to match their corresponding study area.

4. DATA ACCESS

4.1 Sentinel-1 Data

The Synthetic Aperture Radar (SAR) data for this study are from C-band Sentinel-1 returns. Sentinel-1 is part of the European Space Agency's (ESA) Copernicus Program (**https://browser.dataspace.copernicus.eu/**, Accessed Oct. 7, 2025), and has been fully active since 2016 (ESA, 2025). The system is comprised of Sentinel-1A and Sentinel-1B, which are near-polar orbiting and positioned at 180 degrees apart. Sentinel-1B has been out of operation since December 2021.

For this study, Sentinel-1 data were collected in Interferometric Wide Swath (IW) mode at 5x20m resolution and at a 250m swath. Returns occurred at approximately 6:00 and 18:00 local time. The Sentinel-1 dataset used is a Radiometrically Terrain Corrected (RTC) dataset hosted as 32-bit cloud-optimized geotiffs on Microsoft's Planetary Computer (https://planetarycomputer.microsoft.com/dataset/sentinel-1-rtc, Accessed Oct. 7, 2025), and were accessed using a STAC API (Microsoft Open Source et al., 2025). This RTC dataset uses multiple look angles and the 30m PlanetDEM digital elevation model for terrain correction (Small, 2011; Planet Observer, 2017). All polarizations (vv and vh) and multiple incidence angles (29.1 - 46.0 degrees) were used to allow for a more frequent return over each pixel within the study areas (Gagliano et al., 2023). This method increases temporal resolution of Sentinel-1 to approximately 8 days between returns when one satellite was available (starting December 2021, only Sentinel-1A was collecting data) and approximately 5 days when both satellites in the constellation were operational. Using only one polarization or angle caused a decrease in the temporal resolution to 12 or more days (Gagliano et al., 2023), and thus both the vv and vh polarizations and multiple look angles were used. More returns during the melt season are helpful in determining a more precise onset of melt date. For the study sites, the onset of melt date is within a window of 5 to 8 days depending on satellite availability.

4.2 In-Situ Data

In-situ data from the SNOTEL network were used to determine peak SWE dates to compare to the Sentinel-1 onset of snowmelt maps. The National Resource Conservation Service (NRCS) maintains the SNOTEL network, which contains over 800 active sites in the Western United States for monitoring mountain snowpack conditions (Fleming et al., 2023; USDA NRCS, 2025: https://wcc.sc.egov.usda.gov/nwcc/tabget). Daily SWE values were downloaded for each station for the 2021-2025 snow years and filtered to isolate the onset of melt season and find peak SWE.

4.3 Terrain Data

A 10m (1/3 Arc Second) United States Geological Survey (USGS) digital elevation model (DEM) was accessed through the National Map Data Download Application (https://www.usgs.gov/the-national-map-data-delivery/gis-data-download, Accessed Oct. 7, 2025). This DEM was used to obtain elevation data, and compute slope, aspect, and diurnal anisotropic heating (DAH) for the study areas.

4.4 Burn Severity Data

Burn Severity maps for the fires in this study were accessed from the Monitoring Trends in Burn Severity (MTBS) program. This is an interagency program dedicated to assessing landscape and forest conditions post fire (MTBS, 2025). Burn severity maps were developed by calculating the differenced normalized burn ratio (dNBR) for pixels within a fire and assigning thematic class values to them (MTBS Mapping Methods, 2025). MTBS dNBR maps were downloaded from the MTBS data portal (https://mtbs.gov/direct-download, Accessed Oct. 7, 2025).

Table 4.1 Remotely sensed data sources with their units, resolution, and final resolution for this study. The USGS DEM and MTBS dNBR rasters were resampled to the S1 SAR 20m resolution for analysis.

Source	**Type**	**Units**	**Resolution**	**Resolution after resampling**
Sentinel-1	SAR Backscatter	HZ	20m	20m
USGS DEM	Digital Elevation Model	Meters	10m	20m
MTBS	dNBR	Numerical	30m	20m

5. METHODOLOGY

5.1 Sentinel-1 Processing

To calculate runoff onset date, the methodologies outlined in Marin et al. (2020) and Gagliano et al. (2023) were used. These methods identify the date of backscatter minima by iterating through SAR returns within each melt season period (defined as March 01-June 30 to ensure at least 8 returns were captured). Backscatter minima, which is when the most signal from Sentinal-1 is attenuated, occurs when the backscatter is dominated by water, rather than frozen snow, in the return. Because of this, it can be used to determine the first day where liquid water is present in a pixel (onset of melt). In polar environments, seasonal backscatter differencing thresholds between vv and vh polarizations, and a frozen snow reference have been used instead of backscatter minima (Tedesche et al., 2022). However, with larger variations in diurnal temperature fluctuations in the Southern Rocky Mountains, a consistent threshold from a reference "frozen image" had greater variability, and thus the date of backscatter minima was chosen.

Sentinel-1 radiometrically terrain corrected data were queried using the Microsoft Azure ML platform (https://ml.azure.com/, Accessed Oct. 7, 2025), which allows access to Microsoft's RTC S1 dataset. Each year of interest was analyzed separately (2021-2025) using the current version of the Gagliano et al. (2022) Sentinel-1 toolbox (https://github.com/egagli/sar_snowmelt_timing, Accessed Oct. 7, 2025). This code accesses Microsoft's S1 RTC data using the STAC API and iterates through each year (for the purpose of this study, years 2021-2025 melt seasons were assessed) to determine the date of backscatter minima for each pixel within a defined bounding box. A yearly raster is produced with each 20-m resolution pixel as a Julian day of year (DOY) value for the onset of melt. These onset-of-melt rasters were then downloaded for subsequent analysis.

5.2 Sentinel-1 Analysis

The first step of analyzing the DOY rasters was to clip the rectangular bounding boxes defined for querying the Sentinel data for a specific extent from the online platform to the irregular polygonal shape of each fire using the polygon shapefiles of each fire produced by MTBS (https://mtbs.gov/direct-download, Accessed Oct. 7, 2025), which were projected into the coordinate reference system (CRS) WGS UTM Zone 13N (EPSG 3216) using ArcGIS Pro. After clipping each raster to the extent of the corresponding fire, the raster was then filtered to only include pixels with a burn severity of 4, the MTBS thematic indicator for severe burn. Then, each raster was masked by a USGS Digital Elevation Model (DEM), which was resampled from the 10-m native resolution to the 20-m S1 resolution using cubic resampling. From this DEM, the slope, aspect, and northness (sine slope x cosine aspect) (Fassnacht et al., 2012) were calculated for each pixel.

Elevation, northness, and Diurnal Anisotropic Heating (DAH) (Cristea et al., 2017) were the three main variables assessed in this study. Elevations can be used as an assessment of precipitation (Dingman et al., 1988), SWE (Fassnacht et al., 2003), and temperature. When considering melt dynamics, greater amounts of snow require greater energetic inputs to begin melting (Hock, 2003). At higher elevation, temperatures are also colder, meaning onset of melt is delayed (Fassnacht et al., 2017; Harder et al., 2021). For this study, this is an important metric, as temperature is one driver of the onset of snowmelt that can be isolated using elevation. Aspect and slope can be used to calculate northness, which assesses how north facing a pixel is (Cristea et al., 2017). This is important for understanding solar radiative inputs, which play a critical role in the onset of snowmelt in the Southern Rocky Mountains (Marsh et al., 2021; Fassnacht et al., 2017; Reis et al., 2024). Using the onset of melt DOY values along with the terrain variables, each pixels yearly DAH was calculated as a metric for quantifying the amount of solar radiation received by each pixel (Bohner & Antonic, 2009) on the onset of melt date. This calculation has been used previously to better understand the influence of solar radiation in snowmelt timing (Cristea et al., 2017), and for the purposes of this study, was calculated at the 20m resolution of the onset of melt datasets.

Fires were then grouped by year for the assessment of the variability of the onset of snowmelt. To isolate the influence of topographic factors, the data were then aggregated by pixel location to median values across the 5-year period to isolate terrain effects and assess interannual variability. This removes the interannual climate variability and allows for the focus to be specifically on topographic controls. The resulting dataset was then used for further analysis with individual univariate regressions and a multivariate linear regression to examine individual and collocated factors. From the regressions, Pearson coefficients were calculated, as well as unstandardized regression coefficients, which were used to assess the change in onset of melt date per 100 unit increase in elevation or northness.

In addition to completing a regression analysis, spatial autocorrelation was also used to assess spatial timing of the onset of melt. Study areas were filtered to 5,000 pixels using random sampling and then standardized using a z-score for comparison across all fires and years. The Pairwise Euclidean distances between pixel centroids were then calculated, and pixels were then binned into elevation bins. Moran's I values were then calculated for a 500 m distance lag.

Decorrelation distance was then calculated by finding the first distance at which Moran's I dropped below the 0.1 threshold.

Melt synchrony across years was assessed using Pearson correlation, and K-means for spatial clustering. Pixels were grouped in a location-by-year matrix to find locations where there was the same onset of melt DOY across multiple years. Grouped pixels were randomly sampled from each study area. Then, their DOY value and the distance between the two pixels were used to calculate the Pearson correlation between their DOY timeseries. K-means were then used to assess timing patterns based on geographic location and temporal differences. Coordinates and onset of melt DOY were both normalized to a 0-1 scale.

To assess the covariability of elevation and onset of melt date across spatial distance, covariograms for each fire and year were plotted. Traditional variograms assess the spatial autocorrelation of a single variable. Covariograms allow two different variables to co-vary together spatially. This allows for the spatial structure of elevation and onset of melt DOY to be assessed together. Elevation and DOY were both standardized using z-scores to allow for comparison across fires, and distances were binned for consistency. Pixel pairs and the separation distance between them were calculated and used to determine a cross-product of the standardized values. Covariance can then be used to indicate a direct or inverse relationship between elevation and the onset of melt.

5.3 SNOTEL Comparison

The SNOTEL stations nearest to each study area were chosen for comparison to Sentinel results. Peak SWE was selected from the SNOTEL SWE data to compare to the Sentinel-1 onset of snowmelt. Although no SNOTEL sites were not located within the burn areas themselves, they provide information about snow persistence and ablation at the elevation zone that they are in. Many pixels within the high severity burn were at elevations between 2500-3500 m, which is within the elevation zone where most SNOTEL stations are located. The SNOTEL corresponding onset of melt was then compared to S1 derived onset of melt within 100 m of each SNOTEL elevation for each of the five study years.

RESULTS

6.1 Yearly Onset of Melt Distribution and Variability

6.1.1 Melt Distribution

There is defined yearly variability in the distribution of onset of melt dates within each study area (Figure 6.1). Cameron Peak, the largest study area, had moderate variation in the median onset of melt date for the years 2021-2025, with median values ranging between the 99th DOY in 2025 and 111th DOY in 2021. The distribution of onset of melt dates were similar for the years of 2022 and 2025, where data was slightly right skewed, whereas 2021, 2023, and 2024 were slightly left skewed or close to normally distributed.

The East Troublesome Fire, the second largest study area, had less variation in median onset of melt date than Cameron Peak, with median DOY ranging from 108th DOY in 2021 and 2025, to 114th DOY in 2022. All years except for 2023 and 2024, which had a slight left skew, had a slight right skew to the distribution of the data. The Middle Fork Fire across all years tended to have a more consistent distribution than the other fires, with most years having a normal or only slightly left skewed distribution. The median onset of melt date varied between 115th DOY and 127th DOY, making it the study area with the greatest variation in median onset of melt date.

The Mullen Fire had less consistency in distribution count across years, with 2025 standing out as a very right skewed onset of melt. Despite distribution appearing varied, average onset of melt only varied between the 104th DOY and the 113th DOY. Williams Fork fire, the smallest study area, had similar onset of melt date distributions for the 2021 and 2022 melt seasons, and the 2023 and 2024 melt seasons. The 2025 melt season stands out as a very right skewed distribution. Distributions were normal for the 2021, 2022, and 2023 seasons. The median onset of melt date varied between the 99th DOY and 114th DOY (Appendix Table 1).

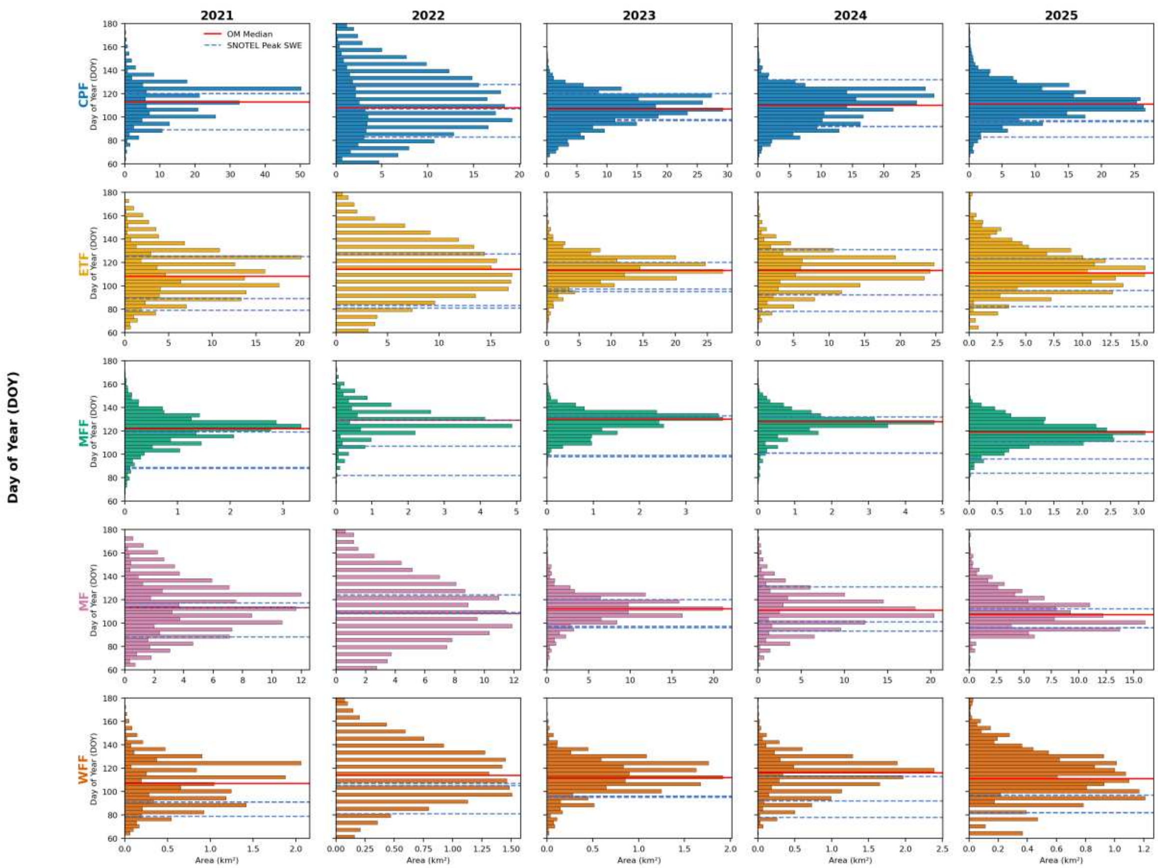

Figure 6.1 Annual histograms of the distribution of onset of melt for all study areas. Bins are color-coded to their study site, and median onset of melt are shown as red dashed lines. The 2 or 3 nearest corresponding SNOTEL station peak SWE dates are shown as dashed blue lines. The x-axis is area in km^2, and the y-axis is day of year.

6.1.2 Interannual Onset of Melt Variability

The interannual variability of the onset of melt for Cameron Peak, East Troublesome, Mullen, and Williams Fork fires were all similar across years (Figure 6.2). The Middle Fork fire stands out consistently as having later onset of melt dates than the other study sites, with median values closer to the 140th DOY (shown in blue). From all the fires, 2025 stands out as having an earlier onset of melt across pixels. This most notable earlier median onset of melt dates in 2025 can be seen in the Cameron Peak, Middle Fork, and Williams Fork study sites (indicated by red pixels).

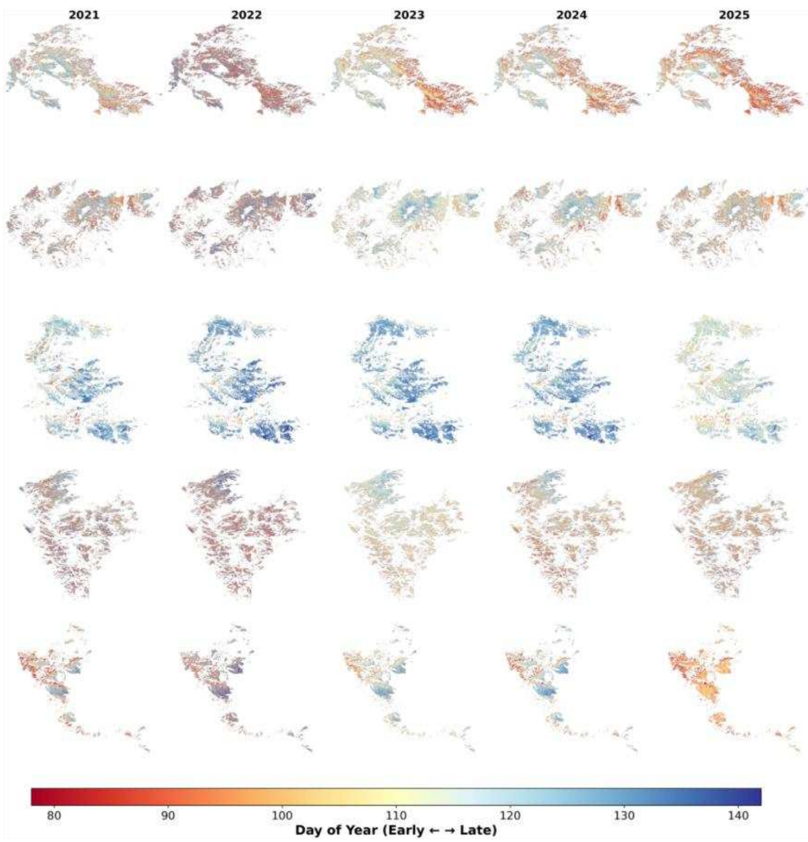

Figure 6.2 Annual onset of melt values for pixels within the high severity areas of each study site. Values ranged from the 60th DOY to the 150th DOY. Earlier onset of melt dates are shown in red, and later onset of melt dates are shown in blue. The Mullen, Cameron Peak, and East Troublesome study areas appear to have less variability from the 5-year median for all years (Figure 6.3).

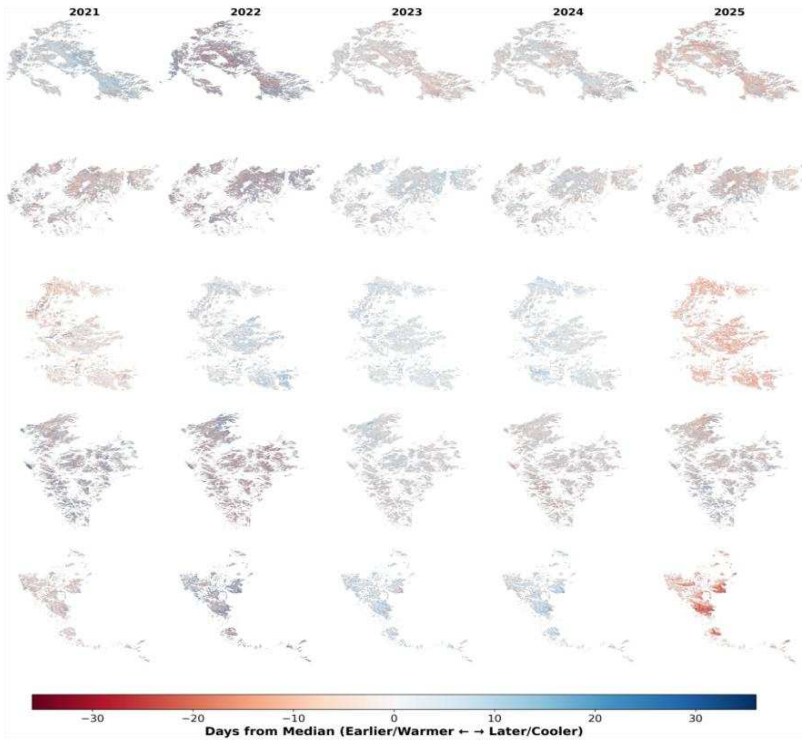

Figure 6.3 Annual differenced rasters between the yearly onset of melt values and the 5-year median for all study sites. Red indicates an earlier, and blue indicates a later onset of melt for that year than the 5-year median.

While there appears to be a visual trend in the onset of melt over the 5-years and the Theil-Sen slope is negative, the Mann-Kendall test shows the decreasing trend to be not significant in the data (Table 6.1). Median DOY values for all fires ranged from the 110th DOY to the 128th DOY (Figure 6.1). Middle Fork Fire consistently has a later median onset of melt for all years, while Cameron Peak had the earliest. When looking at interannual variability, Williams Fork had the most, with a deviation of 6.4 days over the period (Table 6.1).

Table 6.1 Results from interannual variability test using Theil-Sen slope and Mann-Kendall p-values. Based on the results from this analysis, there is no trend in onset of melt over the 5-year period.

Fire	Theil-Sen Slope	Mann-Kendall p-value	Trend	Median DOY	std dev
CPF	0.25	1.00	not significant	110.0	2.39
ETF	-0.25	1.00	not significant	113.0	2.39

MFF	-0.63	0.81	not significant	128.0	4.83
MF	-0.83	0.221	not significant	111.0	2.59
WFF	1.00	0.81	not significant	112.0	3.39

6.2 Topographic Controls on The Onset of Melt

6.2.1 Elevation

When considering terrain variables, elevation had the most correlated effect on the onset of melt dates. Higher elevations have later onset of melt dates across study sites (Figure 6.4a). Per-fire elevation–DOY scatterplots for all pixels are provided in Appendix Figure 2. The range of onset of melt lapse rates for the univariate regression was 2.91 (Cameron Peak Fire) to 5.42 (Mullen Fire) days per 100m of elevation gain, with variations between the study sites. Cameron Peak Fire, which had the greatest elevation range out of all of the study sites, had the smallest effect size at only 2.91 days per 100m of elevation gain (Figure 6.4b). The impact of the temporal resolution of Sentinel-1, i.e., 5 to 8 day returns, can be seen through the sinuous lines of the violin plots (Figures 6.4c and 6.4d). While there was a correlation between higher elevation and later onset of melt DOY, results from the linear regression indicate weak R^2 coefficients across all study areas, with values ranging from 0.034 (Mullen Fire) to 0.13 (Middle Fork Fire).

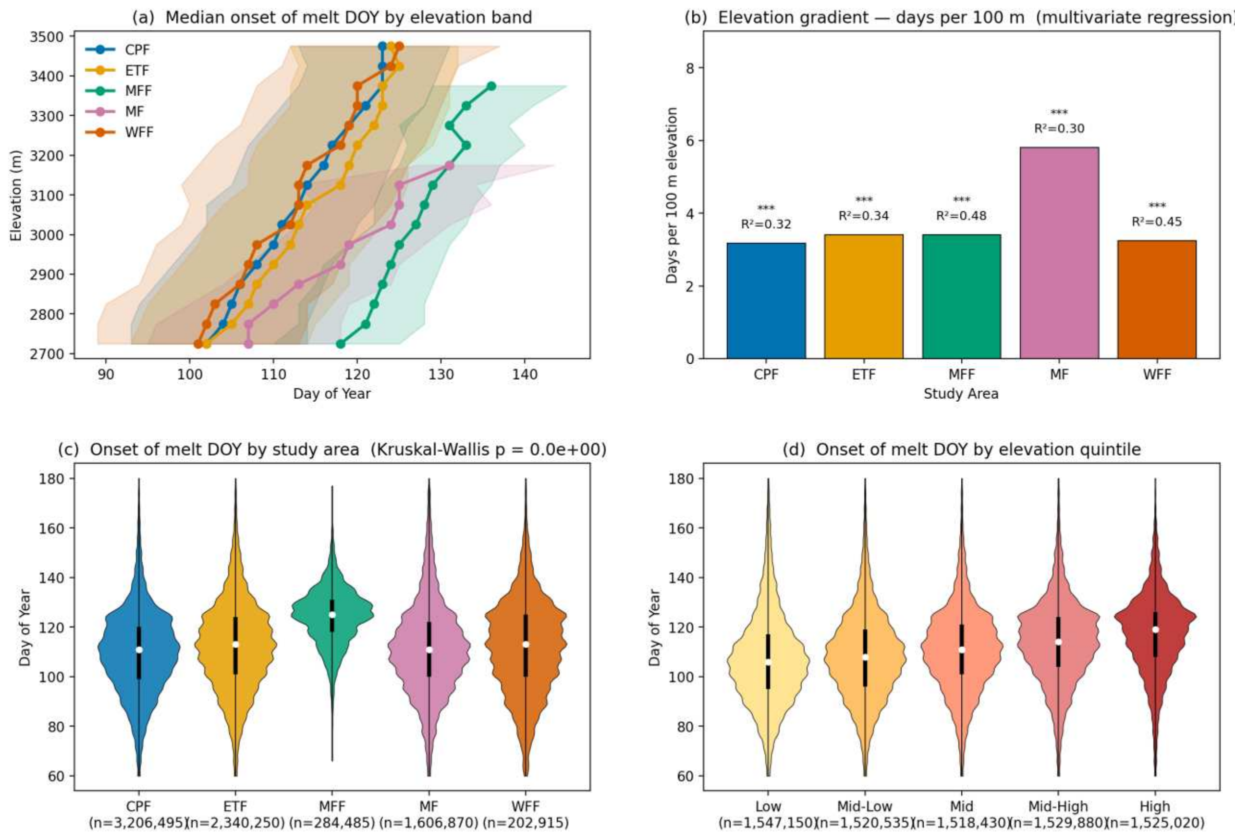

Figure 6.4 Correlation between onset of melt date and elevation as (a) all pixels and median per elevation band versus onset of melt date, (b) mean onset of melt date increases per 100m increase in elevation with R^2 value, (c) distribution of onset of melt date per fire, and (d) distribution of onset of melt date per elevation zone (Appendix Table 3) across all fires .

6.2.2 Northness

When considering "northness" through a univariate regression, the correlation between onset of melt and aspect is less clear, with only the Middle Fork, Williams Fork, and East Troublesome fires illustrating a noticeable correlation. Increased northness leads to later onset of melt date (Figure 6.5). When considering the distribution of aspects within study areas, this weaker correlation becomes more apparent (Figure 6.5). When looking just at the 0.00 to 1.00 northness values, a more consistent correlation can be seen across bins, with values closer to 1.00 having a later onset of melt dates (Figure 6.7).

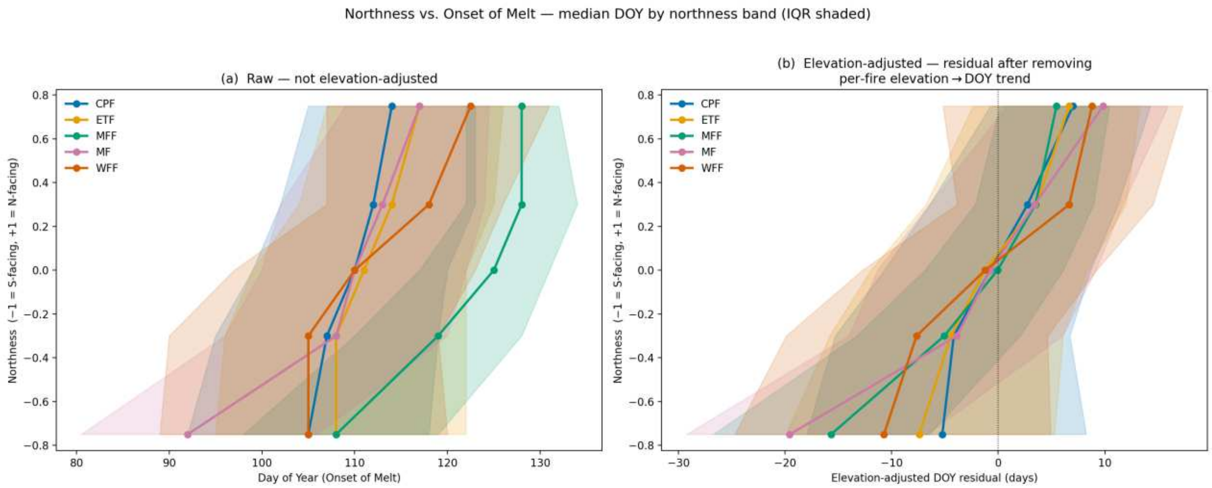

Figure 6.5 Distribution of northness versus onset of melt date, from a univariate regression. (a) Raw relationship (not elevation-adjusted): median onset of melt DOY by northness band, per fire, with the interquartile range shaded. (b) Elevation-adjusted companion panel: DOY residual after removing each fire's own elevation–DOY trend (per-fire linear fit), binned the same way. The northness effect visible in (a) is not purely an elevation artifact — a comparable northness gradient (roughly −10 to +5–10 residual days from south- to north-facing) persists in (b) after elevation is accounted for.

6.2.3 Diurnal Anisotropic Heating

Strong multicollinearity was found between DAH and northness (Figure 6.6). This indicates an inverse relationship, i.e., where northness increases; DAH decreases. A weak correlation can also be seen between slope and DAH. For remaining analysis, only northness was considered an independent variable to remove the multicollinearity and preserve the statistical validity of the regression.

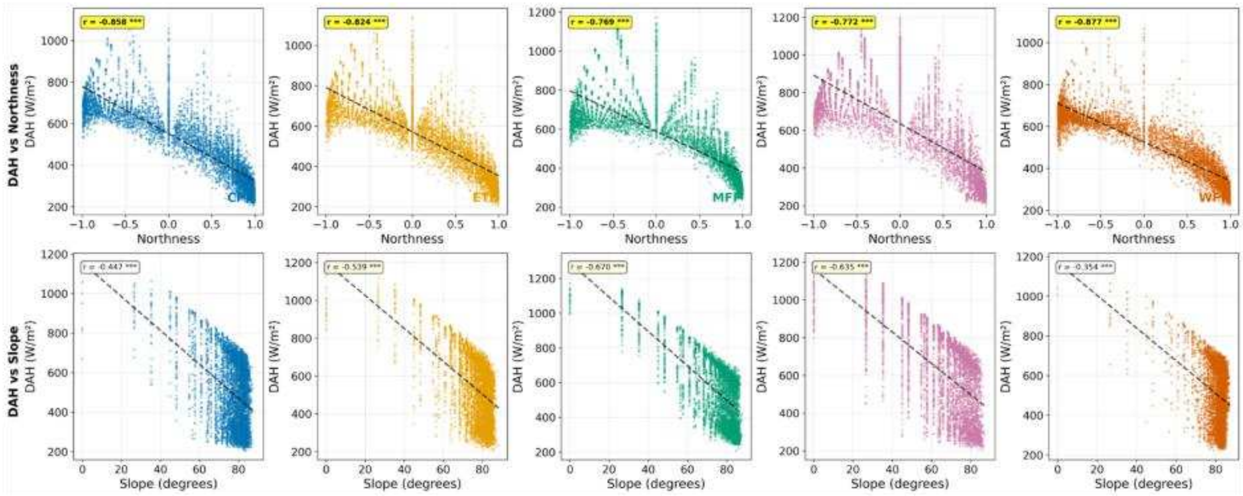

Figure 6.6 Northness and DAH are directly correlated, with consistent trends across all fires. To a smaller extent, DAH and slope are also related.

6.2.4 Multivariate Regression Analysis

The coupled impact of elevation and northness on the onset of melt date is that the onset of melt date occurs latest at high elevations on north facing slopes. The combined multivariate regression has a higher performance than both of the individual univariate regressions, indicating coupled impacts from topographic conditions. Middle Fork Fire had the highest model performance, with an R^2 value of 0.480. When looking at elevation controlling for northness, the effect size of elevation varies between 3.17 to 5.81 days per 100m of elevation gain, a different result from the univariate elevation regression. When assessing northness and controlling elevation, the effect size varies between 15.65 and 24.58 days per unit increase in northness (scale of –1 to 1) (Table 6.2).

Table 6.2 Results from the multivariate linear regression. Non-normalized coefficients for elevation and northness, as well as standard deviation and sample size, are displayed. Significant values ($p < 0.05$) are denoted with an asterisk (*).

Fire	Sample Size	R^2	Elevation Std	Northness Std	Intercept	Elevation Effect Days per 100m	Days per Unit Increase in Northness
CPF	641299	0.325 *	6.52	2.46	13.97	3.17 *	15.65 *

ETF	468050	0.341 *	5.83	2.89	8.75	3.41 *	17.44 *
MF	321374	0.305 *	5.29	1.35	-53.18	5.81 *	19.86 *
MFF	56897	0.480 *	4.83	3.75	22.45	3.40 *	17.40 *
WFF	40583	0.454 *	5.59	5.74	10.38	2.90 *	24.58 *

6.2.5 Spatial Autocorrelation and Clustering

There was limited consistency in spatial autocorrelation across years, with correlation at 500m ranging from 0.045 to 0.288 (Figure 6.7). Mean decorrelation distance varied by study area, from 725m (Williams Fork) to 1,312m (Mullen), with Cameron Peak, East Troublesome, and Middle Fork all averaging roughly 1,075–1,125m (Appendix Figure 3). Looking at cell clustering for onset of melt trends indicates weak correlation for all fires at 500 m spatial distance (Table 6.3). Looking at the variability of the average onset of melt across clusters, the average varied from 42 to 64 days, indicating that there was variability in onset of melt dates of pixels within clusters. The range of DOY values within each cluster varied between 11 days and 24 days (Table 6.3).

Table 6.3 Results from the onset of melt synchrony analysis. Decorrelation distances, Pearson coefficients, timing ranges, and the mean interannual variability all indicate limited spatial autocorrelation across all study sites.

Fire	Mean Autocorr 500m	Std Autocorr 500m	Mean Decorr Distance m	Mean Synchrony	Median Synchrony	N Significant Pairs	Mean Cluster Timing DOY	Timing Range Across Clusters	Mean Interannual Variability
CPF	0.165	0.089	1125	0.073	0.109	397	107	18	61
ETF	0.127	0.060	1075	0.025	0.034	402	111	16	60
MF	0.122	0.056	1312	0.048	0.067	344	110	17	64
MFF	0.178	0.038	1075	0.241	0.310	2281	123	11	54
WFF	0.165	0.063	725	0.220	0.281	3055	108	24	42

While Moran's I value indicate a weak spatial autocorrelation based on pixel location, covariograms for elevation and onset of melt date confirm that the relationship between elevation and onset of melt date is consistent across study areas. At short distances (0-500m) there is a positive covariance value, indicating a strong elevation-onset DOY coupling at a local scale. At farther spatial distances, covariance stays positive, but smaller covariance values indicate a weaker relationship (Figure 6.8). At the farthest spatial distances (5000m) covariance reaches zero or becomes negative, meaning that changes in elevation no longer predict changes in onset of melt DOY (Figure 6.8). Some study areas, such as the Middle Fork and Williams Fork, saw a consistent decay in covariance over spatial distance for all years, while others, such as the Mullen study area which had a slower decay and a less consistent covariance value based on the year (Appendix Figure 10).

Figure 6.7 Gridded matrix of spatial autocorrelation at 500m for all study areas across years. Colors correspond to Morans I values, with greater autocorrelation shown in red, and no or limited autocorrelation is shown in yellow.

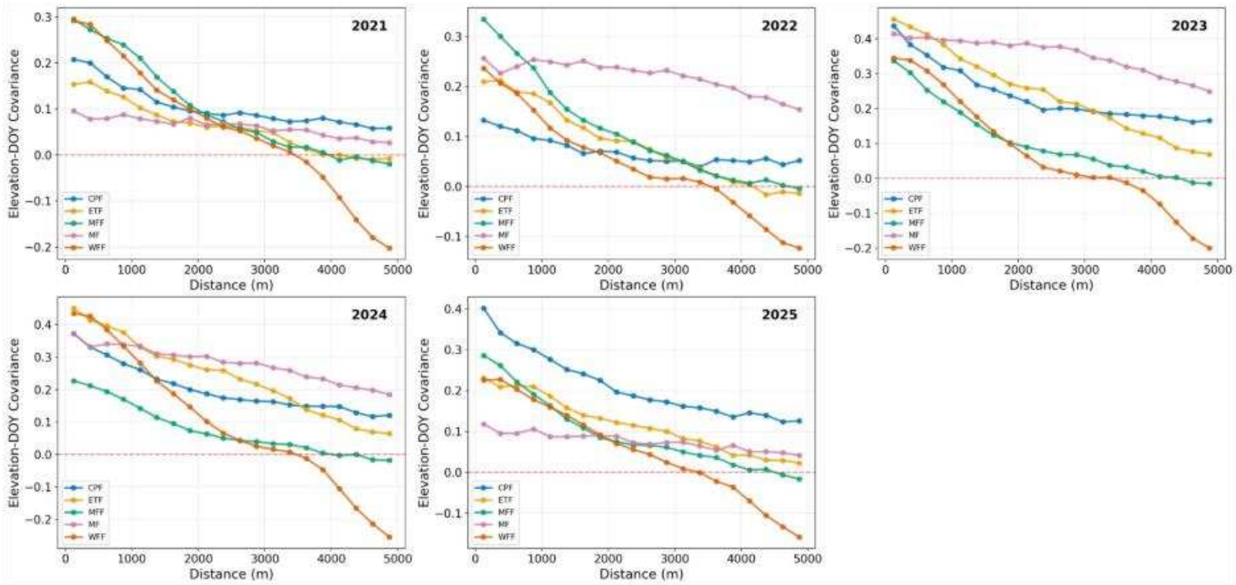

Figure 6.8 Covariograms of elevation-DOY covariance across study areas for each year 2021 to 2025.

6.3 SNOTEL Comparison

For the Cameron Peak Fire, onset of melt dates at pixels near Hourglass Lake were consistently earlier than peak SWE (median OM DOY 105–111 vs. peak SWE DOY 83–120), while pixels near Joe Wright showed onset of melt occurring near or after peak SWE (median OM DOY 117–132 vs. peak SWE DOY 97–132). Melt lag varied by station and year, reflecting local differences in elevation and snow accumulation (Table 6.4). The 5-year mean comparison of S1-derived onset of melt against SNOTEL peak SWE for all five fires is shown in Appendix Figure 9. Note that the SNOTEL peak SWE dates in Figure 6.11a span a wider range (roughly 60 days across stations and years) than the S1-derived onset of melt dates (roughly 15–20 days). This is expected rather than anomalous: each SNOTEL point is a single station-year measurement, while each plotted OM date is the median across several thousand pixels for that fire-year, and medians of large samples are inherently less variable than individual point observations; Sentinel-1's multi-day revisit interval further discretizes the OM dates. The two series are therefore not expected to have comparable spread even where the underlying melt timing is well matched.

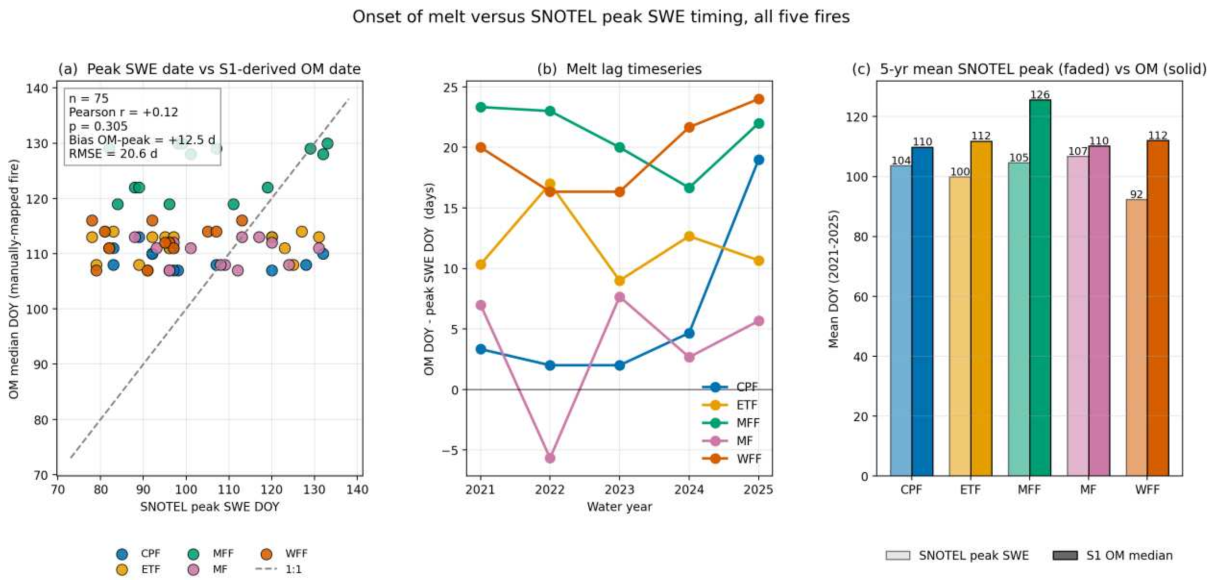

Figure 6.11 Scatterplot of Sentinel-1 derived onset of snowmelt date versus SNOTEL station peak SWE date, melt lag timeseries, and onset melt versus peak SWE bar chart comparison.

Table 6.4 Sentinel-1 derived filtered median onset of melt dates versus corresponding SNOTEL site peak SWE dates. Onset of melt pixels have been filtered to only include cells that are located within 100 m (+ or -) elevation of the corresponding SNOTEL sites. This elevation- and buffer-matched comparison is currently only produced by the pipeline for the Cameron Peak Fire (matched to Hourglass Lake and Joe Wright); rows for the other four fires have been removed from this table because they can no longer be regenerated under the current focus-station configuration (see Section 6.3 methods).For Cameron Peak Fire, pixels were matched to Hourglass Lake and Joe Wright stations within a 2000 m spatial buffer and ±100 m elevation window.

Fire	Year	Median Onset of Melt DOY	SNOTEL Station Name	SNOTEL Peak SWE DOY
Cameron Peak	2021	115	Long Draw Reservoir	119
			Deadman Hill	119
			Joe Wright	118
	2022	108	Long Draw Reservoir	109
			Deadman Hill	125
			Joe Wright	129
	2023	110	Long Draw Reservoir	95
			Deadman Hill	119
			Joe Wright	118
	2024	112	Long Draw Reservoir	100
			Deadman Hill	132

			Joe Wright	131
	2025	105	Long Draw Reservoir	96
			Deadman Hill	95
			Joe Wright	95

7. DISCUSSION AND CONCLUSION

7.1 Onset Melt Distribution and Interannual Variability

The results of this study show variability in the distribution of the onset of melt date across the five high burn severity study sites and all years (Figures 6.1 and 6.2). Several fires exhibited similar onset of melt distributions, such as more left skewed distributions for the 2025 ablation season (Figure 6.1). This is indicative of an earlier trend in the onset of melt, with the East Troublesome, Mullen, and Williams Fork fires seeing the greatest change in distribution. Across all fires, the median onset of melt ranged from the 99th DOY to the 127th DOY (Appendix Table 1). These differences in median onset of melt date are indicative of yearly differences in snowmelt timing, and the variability of onset of melt timing across the study sites.

Looking further into the interannual variability of onset of melt confirms that yearly changes in environment have an impact on snowmelt dynamics in these study sites. When comparing the variability across the study areas, 2025 stands out as consistently deviating from the 5-year median for all study sites (Figure 6.3). This is particularly notable for the Cameron Peak, Middle Fork, and Williams Fork fires, with the 2025 median showing a decrease in onset of melt date across pixels (red pixels in differenced rasters). Williams Fork fire saw the greatest interannual variability overall, which could be due to it being the smallest study area, with even small variation leading to a larger change in median values. Based on the 5-year median, there is a slight trend in earlier onset of melt dates across all study sites (Table 6.1). While this is not a long enough period to be statistically significant, it could be an indicator of changes in the start of ablation season occurring in the Southern Rockies region.

7.2 Impact of Topographic and Geographic Controls

Based on the multivariate analysis, elevation was the greatest topographic driver on the onset of snowmelt for all the study areas and across all years (Table 6.2). The smaller range of the unstandardized regression coefficients confirms a consistent trend in onset of snowmelt across elevations, with an average 3.81 days of delay per 100m elevation gain for all sites (Figure 6.6). This consistent relationship between elevation and onset of melt date is likely related to known correlation between temperature and elevation, and more so the relationship between precipitation and elevation. At higher elevations, there is an increased in precipitation, leading to earlier and longer accumulation of snowpack. This leads to a later onset of melt during the spring months.

While there was a clear relationship between elevation and onset of melt, the relationship between northness and onset of melt date was less clear (Figure 6.7, Table 6.2). There was more variability in the effect of northness on onset of melt date, with a range between 15.65 and 24.58 days per unit increase in northness[2]. This may be due to the nature of each study site having a different range of aspects, with some sites, like Cameron Peak and Middle Fork, having a greater percentage of north-facing pixels within the study areas (Figure 6.5). This would lead to a pixel distribution with a bias towards north facing pixels which could be causing greater variability in onset of melt response due to the uneven distribution of aspects within the study areas.

When thinking about what could be causing this increase in north-facing pixels within the high severity burn pixels of these fires, available fuels could be the cause. In normal years, north-facing areas get the benefit of reduced solar exposure and ample precipitation, allowing for lots of vegetative growth. However, in anomalous years like 2020, prolonged drought periods could turn all of this vegetative growth into fuels. Increase in fuels could lead to a higher severity burn, and therefore a greater distribution of north-facing pixels classified as high severity by MTBS.

Changes in spring conditions year to year could also be impacting the effects of northness on the onset of melt date. Sunnier spring conditions (as opposed to a rainy and cloudy spring) could also lead to a greater difference in solar input between north and south facing pixels. In a spring where cloudier conditions persist, this difference may not be as pronounced.

Because of the less consistent relationship between the onset of snowmelt and pixel northness (Figure 6.7), there was a less clear relationship between onset of melt and diurnal anisotropic heating, even though solar radiation is a known driver of snowmelt in this region. Northness and DAH were found to be directly multicollinear, further confirming why the relationship between elevation and DAH was limited (Appendix Figure 1). For further multivariate analysis, DAH was excluded to account for this direct correlation. While later onset of melt dates within study areas did seem to be related to greater DAH values, this is likely due to seasonal changes in daylight, with days occurring later into the spring/summer months being longer and the sun being higher in the sky, surfaces receive more solar radiation.

7.3 Local Timing Patterns

Looking at more localized spatial trends, the results of the cluster and spatial autocorrelation analysis show that some localized areas may have more similar onset of melt trends than others, but that spatial autocorrelation is limited across all study areas and years (Figure 6.9). Clustering correlation varied across all fires, with Cameron Peak seeing the least variability, and Mullen fire the most (cluster locations and per-cluster DOY distributions for each fire are shown in Appendix Figures 4–8). This could be due to the location of the clusters selected randomly by the algorithm, or due to not all the severely burned pixels within each area being connected. Clusters were also selected from the entirety of the study area, as opposed to being binned by elevation and aspect, which could further increase the spatial variability.

Despite strong topographic controls on the onset of melt (Table 6.2), spatial autocorrelation for individual years at the 500m scale was modest, with fire-level means ranging from 0.12 to 0.18 and individual fire-years reaching as high as 0.29 (Figure 6.9). Autocorrelation was lowest in 2022 (mean 0.08 across fires) and highest in 2023 and 2024 (mean 0.20 in both years) rather than immediately after the fires; this year-to-year pattern does not track a simple post-fire recovery trajectory and warrants further investigation. The result of this analysis indicates that while topography can create a fixed spatial relationship for onset of melt patterns, inter-annual variability created by weather conditions creates substantial stochasticity, leading to reduced spatial autocorrelation.

While Moran's I result indicates weak spatial autocorrelation across study areas and years, the covariogram analysis confirms the relationship between elevation and the onset of melt date across changes in spatial distance. With increases in elevation, the corresponding increase in the onset of melt date can accurately be predicted. While rate of decay varied by study area, the direct relationship between elevation and onset of melt remains true (Figure 6.10). This shows that topography can help in determining, in a relative sense, if a year has an early or late onset of melt. However, weather-specific information could provide an understanding of onset of melt trends in an absolute sense, accounting for both topographic and climatic conditions.

7.4 SNOTEL Comparison

Based on the comparison between the study areas and nearby SNOTEL sites, there was variability in the difference between S-1 derived onset of melt and SNOTEL recorded peak SWE dates. Several fires had median onset of melt dates later than the nearby peak SWE dates. However, Cameron Peak saw the opposite effect, with median onset of melt date occurring before peak SWE at SNOTEL locations. This variability is likely due to study sites covering a wide range of pixels across aspects and locations, while the SNOTEL sites return point data for one location. SNOTEL stations located at lower elevations in relation to their respective study site, such as those close to the East Troublesome and Williams Fork Fires, had a greater difference between the date of peak SWE, and the median onset of melt date.

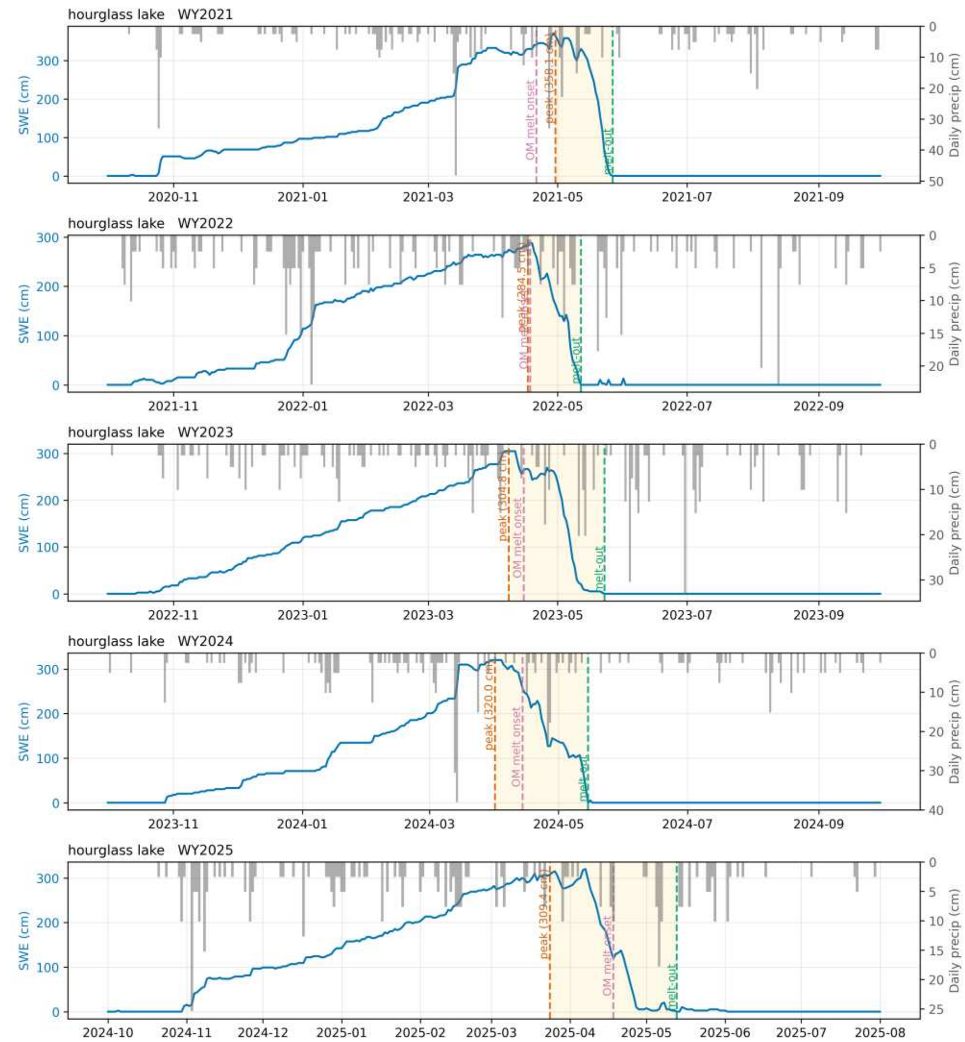

Figure 6.12 Five-year SWE and precipitation traces for Hourglass Lake (water years 2021–2025). Vertical lines mark peak SWE, Sentinel-1 onset-of-melt (median DOY for OM raster pixels matched to this station), and melt-out (first date the station's raw SWE record drops below 1.0 cm following peak). Melt-out is now computed from the raw SWE series rather than the smoothed series used to detect peak and onset, so the marker aligns with where the plotted curve visually reaches zero.

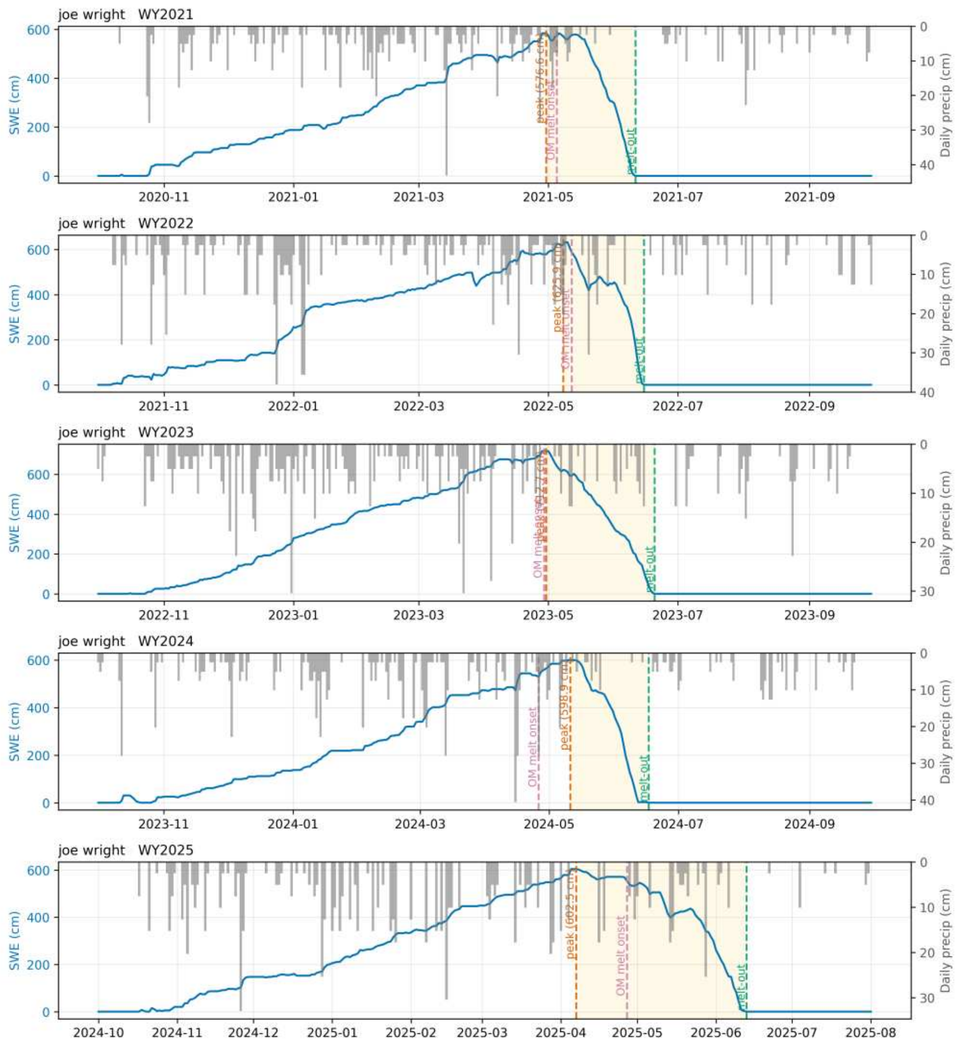

Figure 6.13 Five-year SWE and precipitation traces for Joe Wright (water years 2021–2025), constructed identically to Figure 6.12.

The differences between median onset of melt and peak SWE dates may also indicate that while the SNOTEL network is an excellent source of point data, it may not be representative of the greater area that the station is located in. This may also be due to weather patterns during 5-years within the study period, especially when considering localized trends. Further assessment into the weather conditions that occurred during the study period could give insight into the dynamics of spring conditions at the sites each year.

One further point of interpretation is warranted regarding this lag. It should not be read as the time required for the snowpack to reach an isothermal, "ripe" state after peak SWE: field observations at these sites indicate the snowpack is typically isothermal, or nearly so, well before peak SWE is reached, and SWE itself typically begins to decline once meltwater output is already occurring — i.e., once the pack is already ripe. Two factors tied to how the comparison is constructed, rather than to a physical ripening delay, more plausibly explain the observed lag. First, S-1 onset of melt is compared here to the SNOTEL station's peak SWE date rather than to the station's own melt-onset date; peak SWE marks the end of accumulation, not a melt or ripening event, so some positive offset between it and a later-detected melt signal is expected by construction. Second, the Sentinel-1 onset-of-melt algorithm depends on a C-band backscatter change that requires liquid water content to exceed a detection threshold and persist through the diurnal freeze-thaw cycle, rather than responding to the first appearance of meltwater; because nightly refreezing can continue for some weeks after the pack becomes isothermal, the satellite-detectable signal can lag true internal wetting for reasons unrelated to ripening. Spatial representativeness also contributes: each fire's S-1 median in Figure 6.11 is computed across pixels spanning a range of elevations and aspects, while each SNOTEL station is a single point, so part of the apparent lag reflects higher-elevation, later-melting pixels entering the fire-wide median rather than a lag at any single co-located location. This also explains the apparent inconsistency between Figure 6.11a and Figure 6.11b: the station-year pairs in panel (a) are noisy and not uniformly above the 1:1 line (Pearson $r = 0.12$, RMSE = 20.6 days), while panel (b) plots the mean lag across matched pairs for each fire-year, which smooths over that scatter. The consistently positive appearance of panel (b) is therefore a property of averaging, not evidence that every individual comparison lies above the 1:1 line.

7.5 Future Work

The next steps of this project could focus on upscaling analysis to further look at the predictive nature of terrain features on the onset of melt through a machine learning algorithm, such as RandomForest. This will allow for a more dynamic approach to assessing the statistical power of elevation and northness on the onset of melt in these study areas. Study areas will be divided into smaller subsections to assess local variability and accuracy of the algorithm.

This methodology could also be expanded to other high elevation post-fire study areas to assess geographic, as well as localized differences, in the onset of snowmelt. While this study solely focused on post-fire areas within the Southern Rocky Mountains region, areas within other regions, such as the Northern Rocky Mountains, may also benefit from a similar analysis. With the accessibility of Sentinel-1, this methodology could easily be applied to other areas of interest.

In addition to implementing further statistical techniques, the use of additional remotely sensed data to assess the entirety of the snow season could be implemented. Using an optical satellite such as Sentinel-2 or MODIS would be bene~~i~~ficial for assessing the start of snow persistence and the snow disappearance date for these study areas. In the early stages of this project, the viability of Sentinel-2 optical for the start of snow persistence (SSP) and SDD was assessed and was found to be inaccurate on its own due to cloud cover during the start of accumulation and the end of the ablation seasons, leading to far earlier or later dates than expected. However, utilizing methodology as defined in Revuelto et al., 2021 and Kollert et al., 2024, MODIS, which has a finer temporal resolution, could be downscaled to the spatial resolution of S2 for compatibility with the resolution of these study areas while providing more reliable SSP and SDD dates.

Lastly, while the MTBS dNBR rasters have been widely used to assess burn severity and were beneficial for filtering to only areas with reduced vegetative cover for this study, there are limitations to this methodology. In future, gaps in the canopy, or canopy edge, could be used to define areas of interest using products such as Landsat or S-2 derived Normalized Difference Vegetation Index (NDVI) metrics. This provides a clear understanding of where there is no vegetative cover and increases the accuracy of pixel selection. This methodology has been implemented using airborne LiDAR, which also can offer a finer spatial resolution than spaceborne derived products like MTBS dNBR.

7.6 Conclusion

This study provided insight into onset of snowmelt trends in five high elevation study areas of the Southern Rockies post wildfire. The methodology used in this study confirms the viability of Sentinel-1 to identify the onset of melt date in high severity post-fire landscapes at mid-latitude sites. The Sentinel-1 processing library developed by Gagliano et al. (2023) allowed for the access of data for multiple years and polarizations, expanding the amount of available data, even when only one satellite in the constellation was operational.

Results indicate a strong relationship between the onset of melt and elevation in these study areas, with higher elevations consistently having later onset of melt dates across all fires and years. While study areas covered different ranges in elevation, this trend held consistent across all five locations, indicating a consistent topographic relationship. This was confirmed through a multivariate linear regression and covariogram analysis, where as elevation increased, onset of melt date was delayed. There was also notable variability in onset of melt dates year-to-year, indicating interannual variability impacting onset of melt patterns.

APPENDIX

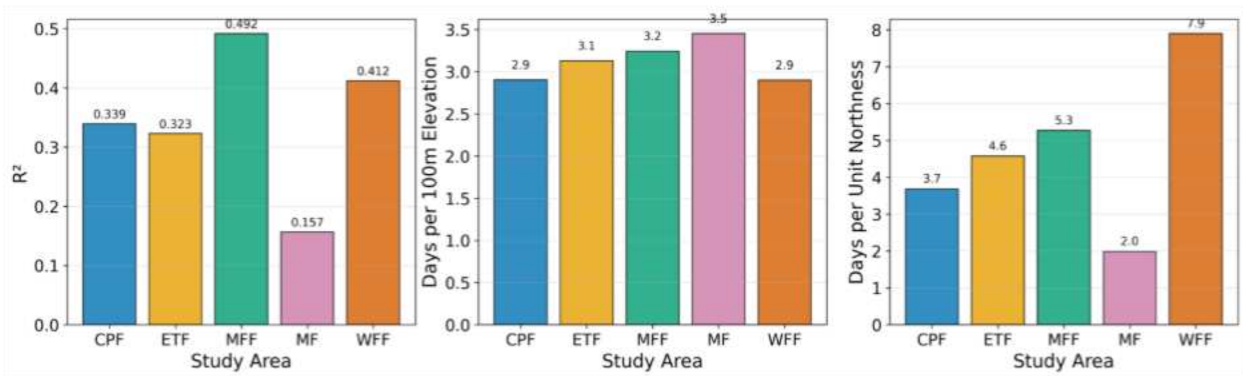

Figure 1. Multivariate linear regression results. Coefficients of determination, as well as effect size for elevation and northness are shown as bar charts for each fire.

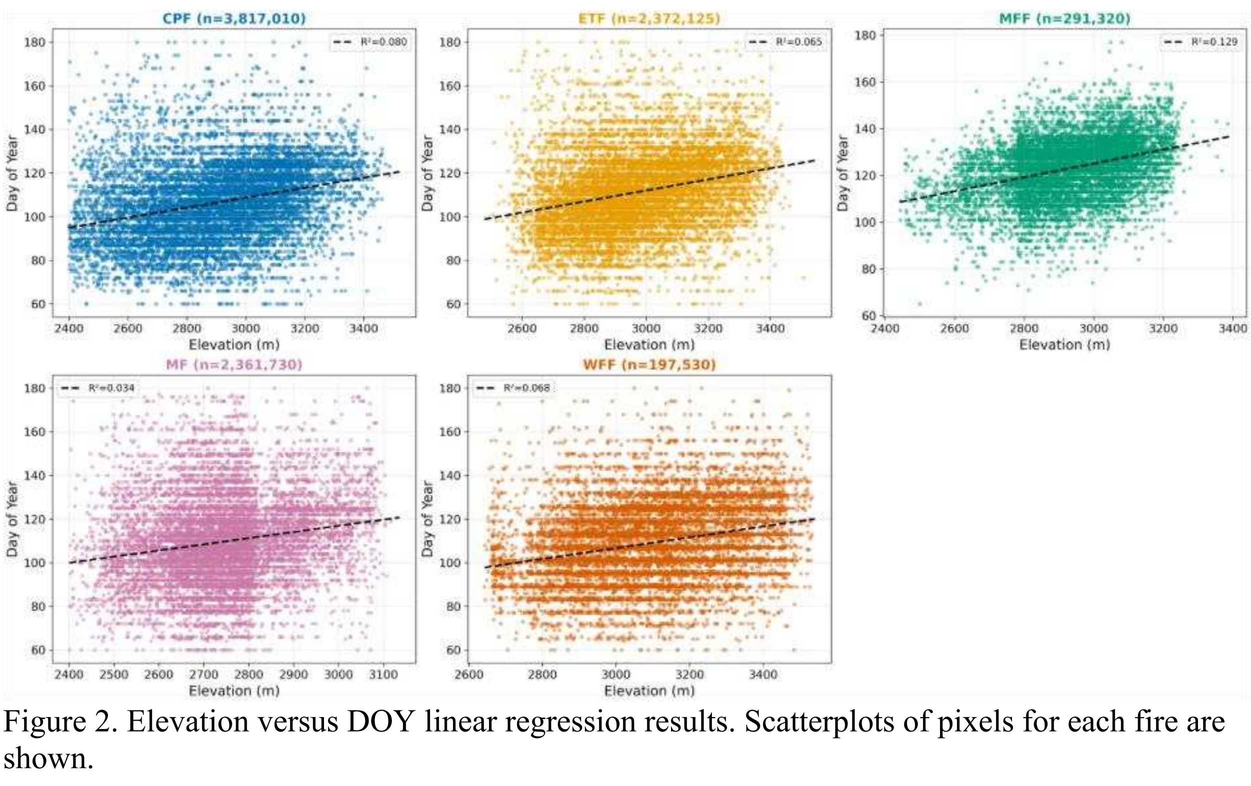

Figure 2. Elevation versus DOY linear regression results. Scatterplots of pixels for each fire are shown.

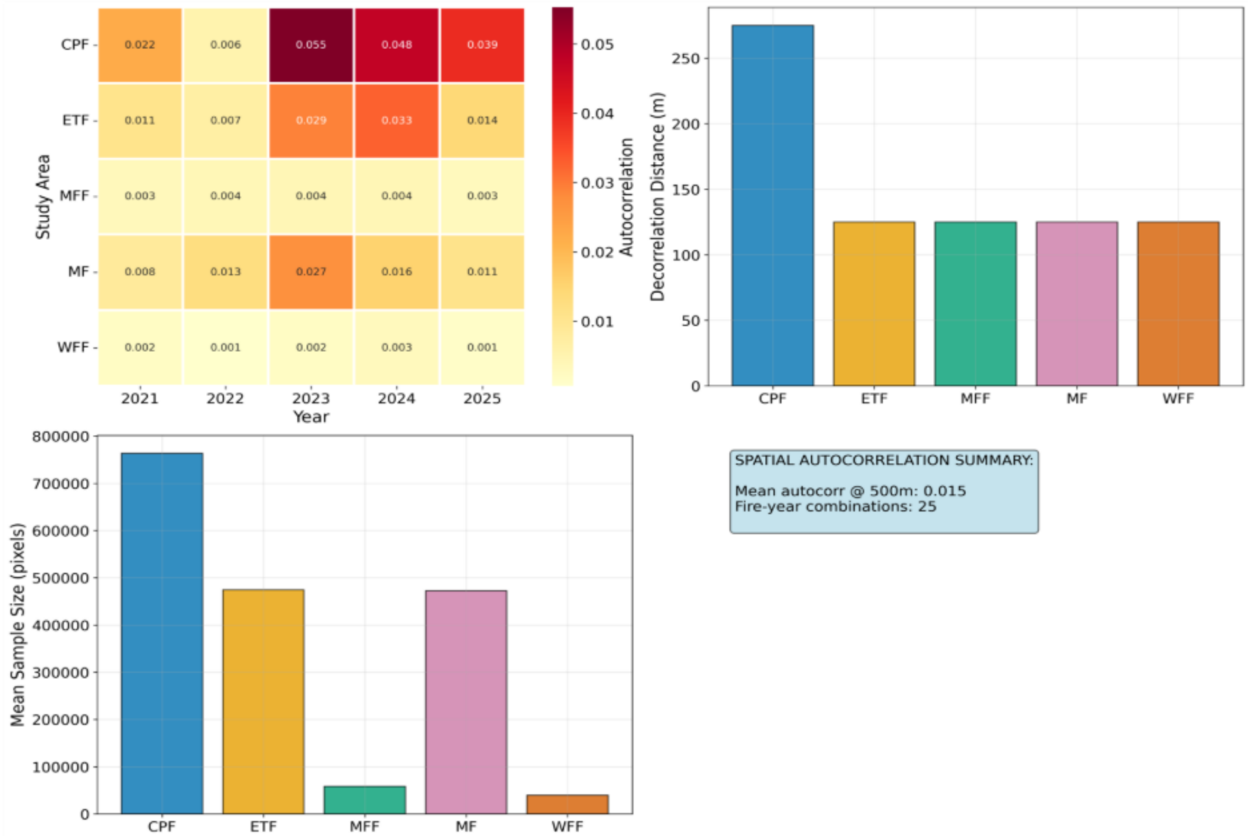

Figure 3. Results from spatial autocorrelation analysis. Gridded matrix, as well as decorrelation distance and sample size, are shown.

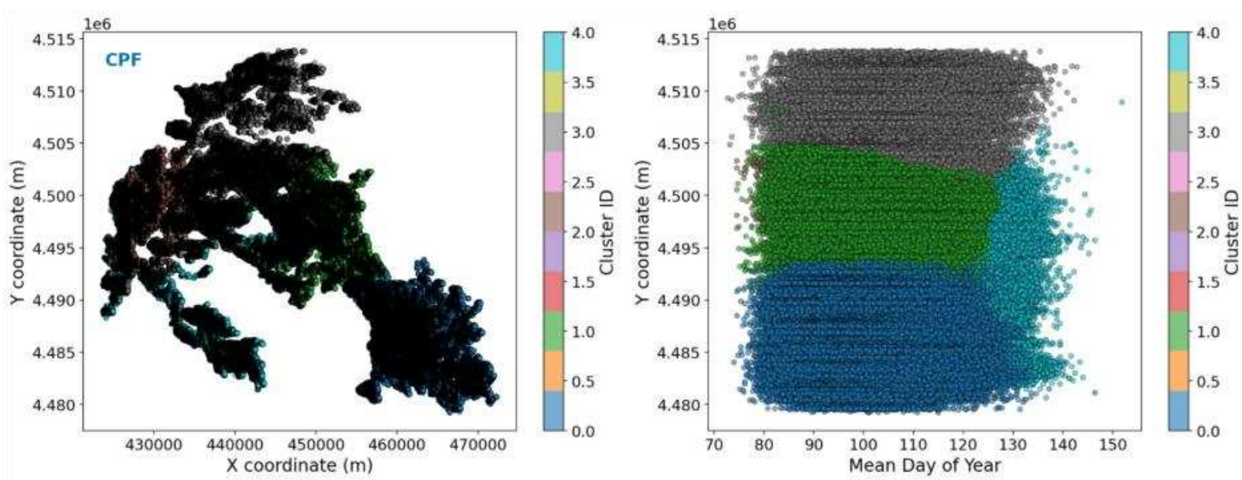

Figure 4. Coordinate clusters used in k-means analysis for Cameron Peak. Cluster locations and DOY value distribution are shown.

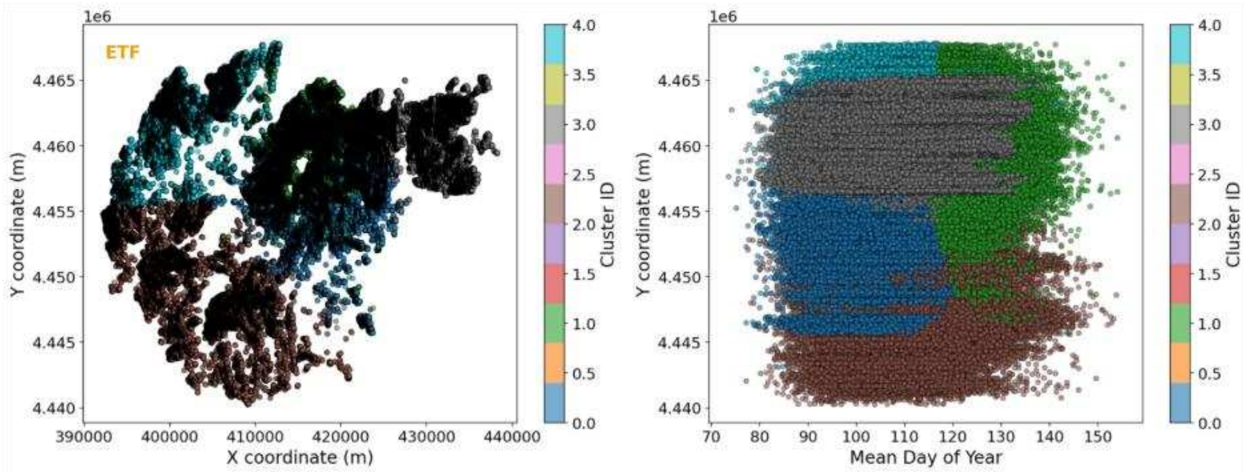

Figure 5. Coordinate clusters used in k-means analysis for East Troublesome. Cluster locations and DOY value distribution are shown.

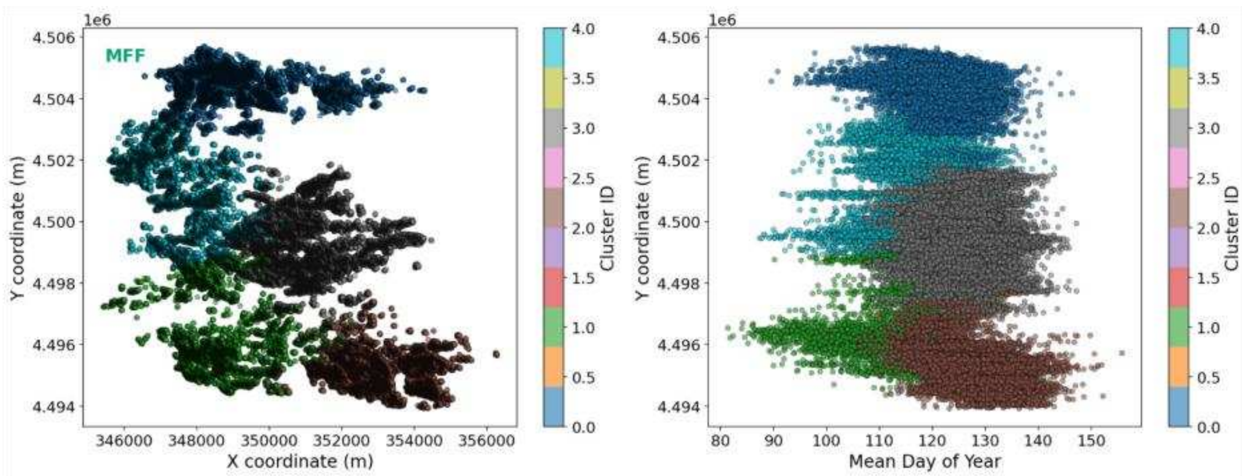

Figure 6. Coordinate clusters used in k-means analysis for Middle Fork. Cluster locations and DOY value distribution are shown.

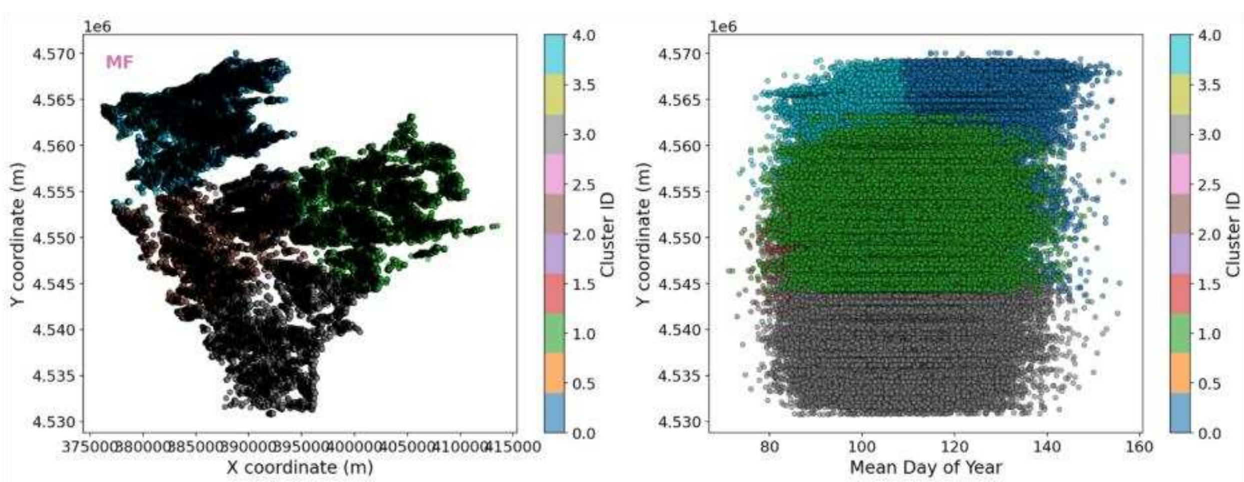

Figure 7. Coordinate clusters used in k-means analysis for Mullen. Cluster locations and DOY value distribution are shown.

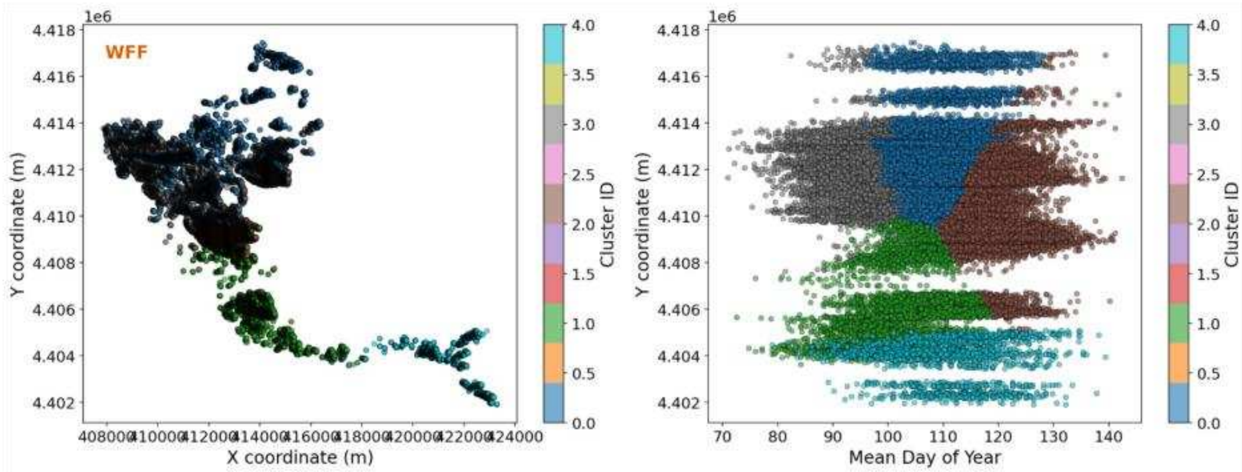

Figure 8. Coordinate clusters used in k-means analysis for Williams Fork. Cluster locations and DOY value distribution are shown.

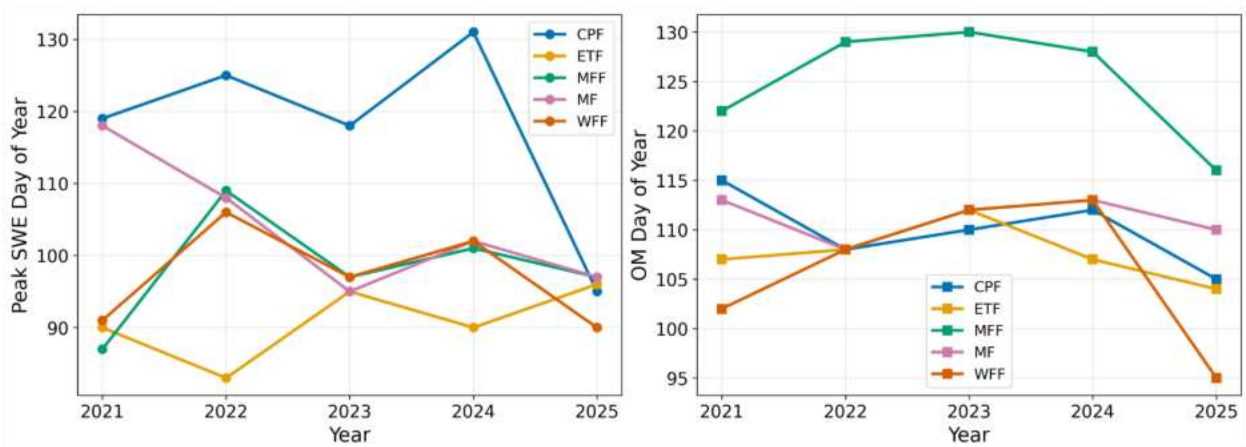

Figure 9. Sentinel-1 derived median onset of melt dates versus SNOTEL median peak SWE for the 5-year period.

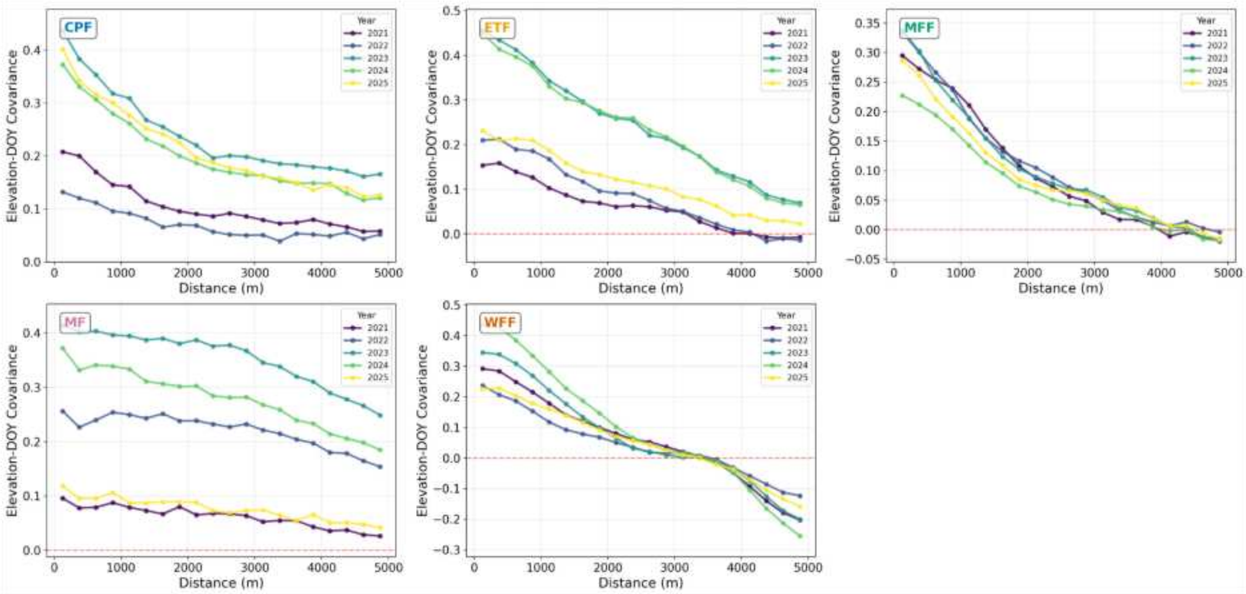

Figure 10. Covariograms for elevation-DOY correlation. Fires are separated into their own figures for comparison between years.

Table 1. Median onset of melt date values for each study area by year.

Fire	Year	Median DOY Value
CPF	2021	113
CPF	2022	108
CPF	2023	107
CPF	2024	110
CPF	2025	111
ETF	2021	108
ETF	2022	114
ETF	2023	113
ETF	2024	113
ETF	2025	111
MFF	2021	122
MFF	2022	129
MFF	2023	130
MFF	2024	128
MFF	2025	119
MF	2021	113
MF	2022	108
MF	2023	112
MF	2024	111
MF	2025	107
WFF	2021	107

WFF	2022	114
WFF	2023	112
WFF	2024	116
WFF	2025	111

Table 2. Elevation bins for multivariate regression analysis with northness. Elevations were binned by pixel medians.

Fire	Min Elevation (m)	Max Elevation (m)	Mean Elevation (m)	Median Elevation (m)	Std Elevation (m)
CPF	2400	3522	2902.54	2913	224.65
ETF	2478	3544	2980.01	2967	186.31
MFF	2442	3392	2932.93	2937	149.05
MF	2400	3136	2745.13	2741	131.23
WFF	2642	3541	3092.01	3092	192.78

Table 3. Elevation bins for spatial autocorrelation analysis. Each study area was separated into 20 bins for grouping clusters.

Fire	Bin Number	Elevation Min (m)	Elevation Max (m)	Bin Width (m)
CPF	1	2399	2456	57
CPF	2	2456	2512	56
CPF	3	2512	2568	56
CPF	4	2568	2624	56
CPF	5	2624	2681	56
CPF	6	2681	2737	56
CPF	7	2737	2793	56
CPF	8	2793	2849	56
CPF	9	2849	2905	56
CPF	10	2905	2961	56
CPF	11	2961	3017	56
CPF	12	3017	3073	56
CPF	13	3073	3129	56
CPF	14	3129	3185	56
CPF	15	3185	3242	56
CPF	16	3242	3298	56
CPF	17	3298	3354	56
CPF	18	3354	3410	56
CPF	19	3410	3466	56
CPF	20	3466	3522	56
ETF	1	2477	2531	54
ETF	2	2531	2585	53
ETF	3	2585	2638	53

ETF	4	2638	2691	53
ETF	5	2691	2745	53
ETF	6	2745	2798	53
ETF	7	2798	2851	53
ETF	8	2851	2904	53
ETF	9	2904	2958	53
ETF	10	2958	3011	53
ETF	11	3011	3064	53
ETF	12	3064	3118	53
ETF	13	3118	3171	53
ETF	14	3171	3224	53
ETF	15	3224	3278	53
ETF	16	3278	3331	53
ETF	17	3331	3384	53
ETF	18	3384	3437	53
ETF	19	3437	3491	53
ETF	20	3491	3544	53
MFF	1	2441	2490	48
MFF	2	2490	2537	48
MFF	3	2537	2585	48
MFF	4	2585	2632	48
MFF	5	2632	2680	48
MFF	6	2680	2727	48
MFF	7	2727	2775	48
MFF	8	2775	2822	48
MFF	9	2822	2870	48
MFF	10	2870	2917	48
MFF	11	2917	2965	48
MFF	12	2965	3012	48
MFF	13	3012	3060	48
MFF	14	3060	3107	48
MFF	15	3107	3155	48
MFF	16	3155	3202	48
MFF	17	3202	3250	48
MFF	18	3250	3297	48
MFF	19	3297	3345	48
MFF	20	3345	3392	48
MF	1	2399	2437	38
MF	2	2437	2474	37
MF	3	2474	2510	37
MF	4	2510	2547	37

MF	5	2547	2584	37
MF	6	2584	2621	37
MF	7	2621	2658	37
MF	8	2658	2694	37
MF	9	2694	2731	37
MF	10	2731	2768	37
MF	11	2768	2805	37
MF	12	2805	2842	37
MF	13	2842	2878	37
MF	14	2878	2915	37
MF	15	2915	2952	37
MF	16	2952	2989	37
MF	17	2988.8	3026	37
MF	18	3026	3062	37
MF	19	3062	3099	37
MF	20	3099	3136	37
WFF	1	2641	2687	46
WFF	2	2687	2732	45
WFF	3	2732	2777	45
WFF	4	2777	2822	45
WFF	5	2822	2867	45
WFF	6	2867	2912	45
WFF	7	2912	2957	45
WFF	8	2957	3002	45
WFF	9	3002	3047	45
WFF	10	3047	3092	45
WFF	11	3092	3136	45
WFF	12	3136	3181	45
WFF	13	3181	3226	45
WFF	14	3226	3271	45
WFF	15	3271	3316	45
WFF	16	3316	3361	45
WFF	17	3361	3406	45
WFF	18	3406	3451	45
WFF	19	3451	3496	45
WFF	20	3496	3541	45

Table 3. Numerical bins used in the multivariate regression analysis for trends in onset of melt and elevation across fires. Results were displayed as a violin plot in the results chapter.

Fire	**Elevation Category**	**Min Elevation (m)**	**Max Elevation (m)**	**Mean Elevation (m)**	**Median Elevation (m)**	**Std Elevation (m)**	**Bin Width (m)**

CPF	Low	2400	2696	2577	2588	81.55	296
CPF	Mid-Low	2697	2851	2778	2779	44.80	154
CPF	Mid	2852	2975	2914	2914	35.55	123
CPF	Mid-High	2976	3104	3038	3037	37.20	128
CPF	High	3105	3522	3209	3188	83.71	417
ETF	Low	2478	2813	2727	2738	62.17	335
ETF	Mid-Low	2814	2917	2869	2871	29.63	103
ETF	Mid	2918	3023	2969	2968	30.75	105
ETF	Mid-High	3024	3155	3086	3085	37.88	131
ETF	High	3156	3544	3252	3241	67.94	388
MFF	Low	2442	2809	2721	2755	86.32	367
MFF	Mid-Low	2810	2893	2853	2854	24.27	83
MFF	Mid	2894	2984	2938	2938	27.15	90
MFF	Mid-High	2985	3065	3025	3024	22.91	80
MFF	High	3066	3392	3131	3118	50.96	326
MF	Low	2400	2642	2567	2575	55.93	242
MF	Mid-Low	2643	2713	2680	2681	20.48	70
MF	Mid	2714	2769	2742	2742	16.22	55
MF	Mid-High	2770	2846	2797	2793	19.38	76
MF	High	2847	3136	2942	2929	65.64	289
WFF	Low	2642	2916	2823	2842	72.58	274
WFF	Mid-Low	2917	3037	2979	2981	34.05	120
WFF	Mid	3038	3142	3092	3093	30.66	104
WFF	Mid-High	3143	3272	3201	3198	37.81	129
WFF	High	3273	3541	3368	3360	63.87	268

REFERENCES

Addington, R. N., Aplet, G. H., Battaglia, M. A., Briggs, J. S., Brown, P. M., Cheng, A. S., Dickinson, Y., Feinstein, J. A., Pelz, K. A., Regan, C. M., Thinnes, J., Truex, R., Fornwalt, P. J., Gannon, B., Julian, C. W., Underhill, J. L., & Wolk, B. (2018). *Principles and Practices for the Restoration of Ponderosa Pine and Dry Mixed-Conifer Forests of the Colorado Front Range*. https://doi.org/10.2737/rmrs-gtr-373

Abatzoglou, J. T., & Williams, A. P. (2016). Impact of anthropogenic climate change on wildfire across western US forests. *Proceedings of the National Academy of Sciences*, *113*(42), 11770–11775. https://doi.org/10.1073/pnas.1607171113

Agee, J. K., & Skinner, C. N. (2005). Basic principles of forest fuel reduction treatments. *Forest Ecology and Management*, *211*(1–2), 83–96. https://doi.org/10.1016/j.foreco.2005.01.034

Alizadeh, M. R., Abatzoglou, J. T., Luce, C. H., Adamowski, J. F., Farid, A., & Sadegh, M. (2021). Warming enabled upslope advance in western US forest fires. *Proceedings of the National Academy of Sciences*, *118*(22), e2009717118. https://doi.org/10.1073/pnas.2009717118

Allen, C. D., Savage, M., Falk, D. A., Suckling, K. F., Swetnam, T. W., Schulke, T., Stacey, P. B., Morgan, P., Hoffman, M., & Klingel, J. T. (2002). Ecological Restoration of Southwestern Ponderosa Pine Ecosystems: A Broad Perspective. *Ecological Applications*, *12*(5), 1418–1433. https://doi.org/10.1890/1051-0761(2002)012[1418:EROSPP]2.0.CO;2

Amatulli, G., McInerney, D., Sethi, T., Strobl, P., & Domisch, S. (2020). Geomorpho90m, empirical evaluation and accuracy assessment of global high-resolution geomorphometric layers. *Scientific Data*, *7*, 162. https://doi.org/10.1038/s41597-020-0479-6

An evaluation of terrain-based downscaling of fractional snow covered area data sets based on LiDAR-derived snow data and orthoimagery—Cristea—2017—Water Resources Research—Wiley Online Library. (n.d.). Retrieved February 1, 2024, from https://agupubs.onlinelibrary.wiley.com/doi/10.1002/2017WR020799

Anthony LeRoy Westerling. (n.d.). *Increasing western US forest wildfire activity: Sensitivity to changes in the timing of spring*. https://doi.org/10.1098/rstb.2015.0178

Aragon, C. M., & Hill, D. F. (2024). Changing snow water storage in natural snow reservoirs. *Hydrology and Earth System Sciences*, *28*(4), 781–800. https://doi.org/10.5194/hess-28-781-2024

Armstrong, A., Tassone, M., & Braaten, J. (2024). Defining Seasonality: First Date of No Snow. In J. A. Cardille, M. A. Crowley, D. Saah, & N. E. Clinton (Eds.), *Cloud-Based Remote Sensing* *with Google Earth Engine: Fundamentals and Applications* (pp. 985–1001). Springer International Publishing. https://doi.org/10.1007/978-3-031-26588-4_45

Automated Snow Monitoring. (n.d.). Retrieved September 4, 2024, from https://www.nrcs.usda.gov/wps/portal/wcc/home/aboutUs/monitoringPrograms/automatedSnowMonitoring/

Baker, W. L. (2018). Historical fire regimes in ponderosa pine and mixed-conifer landscapes of the San Juan Mountains, Colorado, USA, from multiple sources. *Fire*, *1*(2), 23. https://doi.org/10.3390/fire1020023

Bales, R. C., Dressler, K. A., Imam, B., Fassnacht, S. R., & Lampkin, D. (2008). Fractional snow cover in the Colorado and Rio Grande basins, 1995–2002. *Water Resources Research*, *44*(1). https://doi.org/10.1029/2006WR005377

Barber, D. G., Iacozza, J., & Walker, A. E. (2002). On the estimation of snow water equivalent (SWE) using microwave radiometry over Arctic first-year sea ice. *IEEE International Geoscience and Remote Sensing Symposium*, *5*, 3050–3052 vol.5. https://doi.org/10.1109/IGARSS.2002.1026866

Barbero, R., Abatzoglou, J. T., Larkin, N. K., Kolden, C. A., & Stocks, B. (2015). Climate change presents increased potential for very large fires in the contiguous United States. *International Journal of Wildland Fire*, *24*(7), 892–899. https://doi.org/10.1071/WF15083

Barnett, T. P., Adam, J. C., & Lettenmaier, D. P. (2005). Potential impacts of a warming climate on water availability in snow-dominated regions. *Nature*, *438*(7066), Article 7066. https://doi.org/10.1038/nature04141

Barnhart, T. B., Tague, C. L., & Molotch, N. P. (2020). The Counteracting Effects of Snowmelt Rate and Timing on Runoff. *Water Resources Research*, *56*(8), e2019WR026634. https://doi.org/10.1029/2019WR026634

Battaglia, M. A., Gannon, B., Brown, P. M., Fornwalt, P. J., Cheng, A. S., & Huckaby, L. S. (2018). Changes in forest structure since 1860 in Ponderosa pine dominated forests in the Colorado and Wyoming front range, USA. *Forest Ecology and Management*, *422*, 147–160. https://doi.org/10.1016/j.foreco.2018.04.010

Bazzi, H., Baghdadi, N., Nino, P., Napoli, R., Najem, S., Zribi, M., & Vaudour, E. (2023). Retrieving soil moisture from sentinel-1: Limitations over certain crops and sensitivity to the first soil thin layer. *Water*, *16*(1), 40. https://doi.org/10.3390/w16010040

Bertone, A., Zucca, F., Marin, C., Notarnicola, C., Cuozzo, G., Krainer, K., Mair, V., Riccardi, P., Callegari, M., & Seppi, R. (2019). An Unsupervised Method to Detect Rock Glacier Activity by Using Sentinel-1 SAR Interferometric Coherence: A Regional-Scale Study in the Eastern European Alps. *Remote Sensing*, *11*(14), Article 14. https://doi.org/10.3390/rs11141711

Bladon, K. D., Emelko, M. B., Silins, U., & Stone, M. (2014). Wildfire and the future of Water Supply. *Environmental Science & Technology*, *48*(16), 8936–8943. https://doi.org/10.1021/es500130g

Bonnell, R. (2024, May 22). *A Warmer Spring: How a Changing Snowpack is Altering Colorado's Environment*. Colorado State University. https://sustainability.colostate.edu/humannature/changing-snowpack-is-altering-colorados-environment/

Brown, T. C., Mahat, V., & Ramirez, J. A. (2019). Adaptation to future water shortages in the United States caused by population growth and climate change. *Earth's Future*, *7*(3), 219–234. https://doi.org/10.1029/2018ef001091

Buchelt, S., Skov, K., Rasmussen, K. K., & Ullmann, T. (2022). Sentinel-1 time series for mapping snow cover depletion and timing of snowmelt in Arctic periglacial environments: Case study from Zackenberg and Kobbefjord, Greenland. *The Cryosphere*, *16*(2), 625–646. https://doi.org/10.5194/tc-16-625-2022

Burles, K., & Boon, S. (2011). Snowmelt energy balance in a burned forest plot, Crowsnest Pass, Alberta, Canada. *Hydrological Processes*, *25*(19), 3012–3029. https://doi.org/10.1002/hyp.8067

Busby, S. U., Moffett, K. B., & Holz, A. (2020). High-severity and short-interval wildfires limit forest recovery in the Central Cascade Range. *Ecosphere*, *11*(9). https://doi.org/10.1002/ecs2.3247

Chang, A. T. C., Foster, J. L., & Hall, D. K. (1987). Nimbus-7 SMMR Derived Global Snow Cover Parameters. *Annals of Glaciology*, *9*, 39–44. https://doi.org/10.3189/S0260305500200736

Che, T., Li, X., Jin, R., Armstrong, R., & Zhang, T. (2008). Snow depth derived from passive microwave remote-sensing data in China. *Annals of Glaciology*, *49*, 145–154. https://doi.org/10.3189/172756408787814690

Clifford, D. (2010). Global estimates of snow water equivalent from passive microwave instruments: History, challenges and future developments. *International Journal of Remote Sensing*, *31*(14), 3707–3726. https://doi.org/10.1080/01431161.2010.483482

Climate and wildfire area burned in western U.S. ecoprovinces, 1916–2003—Littell—2009—Ecological Applications—Wiley Online Library. (n.d.). Retrieved September 4, 2024, from https://esajournals.onlinelibrary.wiley.com/doi/10.1890/07-1183.1

Clow, D. W. (2010). *Changes in the Timing of Snowmelt and Streamflow in Colorado: A Response to Recent Warming*. https://doi.org/10.1175/2009JCLI2951.1

Copernicus Sentinel-2A Calibration and Products Validation Status. (n.d.). Retrieved October 3, 2024, from https://www.mdpi.com/2072-4292/9/6/584

Collados-Lara, A., Fassnacht, S. R., Pulido-Velazquez, D., Pfohl, A. K. D., Morán-Tejeda, E., Venable, N. B. H., Pardo-Igúzquiza, E., & Puntenney-Desmond, K. (2020). Intra-day variability of temperature and its near-surface gradient with elevation over mountainous terrain: Comparing MODIS land surface temperature data with coarse and fine scale near-surface measurements. *International Journal of Climatology*, *41*(S1). https://doi.org/10.1002/joc.6778

Colorado's forest types. Colorado State Forest Service. (2025, July 14). https://csfs.colostate.edu/forests-trees/forest-types/

Cordisco, E., Prigent, C., & Aires, F. (2006). Snow characterization at a global scale with passive microwave satellite observations. *Journal of Geophysical Research: Atmospheres*, *111*(D19). https://doi.org/10.1029/2005JD006773

Cui, G., Anderson, M., & Bales, R. (2023). Runoff response to the uncertainty from key water-budget variables in a seasonally snow-covered mountain basin. *Journal of Hydrology: Regional Studies*, *50*, 101601. https://doi.org/10.1016/j.ejrh.2023.101601

Daly, S. F., Davis, R., Ochs, E., & Pangburn, T. (2000). An approach to spatially distributed snow modelling of the Sacramento and San Joaquin Basins, California. *Hydrological Processes*, *14*(18), 3257–3271. https://doi.org/10.1002/1099-1085(20001230)14:18<3257::aid-hyp199>3.0.co;2-z

Darychuk, S., Shea, J., Menounos, B., Chesnokova, A., Jost, G., & Weber, F. (2023). Snowmelt characterization from optical and synthetic-aperture radar observations in the La Joie Basin, British Columbia. *The Cryosphere*, *17*, 1457–1473. https://doi.org/10.5194/tc-17-1457-2023

Davis, K. T., Robles, M. D., Kemp, K. B., Higuera, P. E., Chapman, T., Metlen, K. L., Peeler, J. L., Rodman, K. C., Woolley, T., Addington, R. N., Buma, B. J., Cansler, C. A., Case, M. J., Collins, B. M., Coop, J. D., Dobrowski, S. Z., Gill, N. S., Haffey, C., Harris, L. B., … Campbell, J. L. (2023). Reduced fire severity offers near-term buffer to climate-driven declines in conifer resilience across the western United States. *Proceedings of the National Academy of Sciences*, *120*(11). https://doi.org/10.1073/pnas.2208120120

Deacon, J. E., Williams, A. E., Williams, C. D., & Williams, J. E. (2007). Fueling population growth in Las Vegas: How large-scale groundwater withdrawal could burn regional biodiversity. *BioScience*, *57*(8), 688–698. https://doi.org/10.1641/b570809

Dennison, P. E., Brewer, S. C., Arnold, J. D., & Moritz, M. A. (2014). Large wildfire trends in the western United States, 1984–2011. *Geophysical Research Letters*, *41*(8), 2928–2933. https://doi.org/10.1002/2014GL059576

Derksen, C., Walker, A., & Goodison, B. (2005). Evaluation of passive microwave snow water equivalent retrievals across the boreal forest/tundra transition of western Canada. *Remote Sensing of Environment*, *96*(3), 315–327. https://doi.org/10.1016/j.rse.2005.02.014

Development of methods for mapping global snow cover using moderate resolution imaging spectroradiometer data—ScienceDirect. (n.d.). Retrieved September 5, 2024, from https://www.sciencedirect.com/science/article/pii/003442579500137P?via%3Dihub

Dietz, A. J., Kuenzer, C., Gessner, U., & Dech, S. (2012). Remote sensing of snow – a review of available methods. *International Journal of Remote Sensing*, *33*(13), 4094–4134. https://doi.org/10.1080/01431161.2011.640964

Dillon, G. K., Holden, Z. A., Morgan, P., Crimmins, M. A., Heyerdahl, E. K., & Luce, C. H. (2011). Both topography and climate affected forest and woodland burn severity in two regions of the western US, 1984 to 2006. *Ecosphere*, *2*(12). https://doi.org/10.1890/es11-00271.1

Does Sentinel-1A Backscatter Capture the Spatial Variability in Canopy Gaps of Tropical Agroforests? A Proof-of-Concept in Cocoa Landscapes in Cameroon. (n.d.). X-Mol.Net. Retrieved February 25, 2024, from https://www.x-mol.net/paper/article/1340520950681747456

Dozier, J. (1989). Spectral signature of alpine snow cover from the landsat thematic mapper. *Remote Sensing of Environment*, *28*, 9–22. https://doi.org/10.1016/0034-4257(89)90101-6

Dozier, J., & Painter, T. H. (2004). MULTISPECTRAL AND HYPERSPECTRAL REMOTE SENSING OF ALPINE SNOW PROPERTIES. *Annual Review of Earth and Planetary Sciences*, *32*(Volume 32, 2004), 465–494. https://doi.org/10.1146/annurev.earth.32.101802.120404

Dressler, K. A., Leavesley, G. H., Bales, R. C., & Fassnacht, S. R. (2006). Evaluation of gridded snow water equivalent and satellite snow cover products for mountain basins in a hydrologic model. *Hydrological Processes*, *20*(4), 673–688. https://doi.org/10.1002/hyp.6130

Drusch, M., Del Bello, U., Carlier, S., Colin, O., Fernandez, V., Gascon, F., Hoersch, B., Isola, C., Laberinti, P., Martimort, P., Meygret, A., Spoto, F., Sy, O., Marchese, F., & Bargellini, P. (2012). Sentinel-2: ESA's optical high-resolution mission for GMES Operational Services. *Remote Sensing of Environment*, *120*, 25–36. https://doi.org/10.1016/j.rse.2011.11.026

Dubois, C., Mueller, M. M., Pathe, C., Jagdhuber, T., Cremer, F., Thiel, C., & Schmullius, C. (2020). CHARACTERIZATION OF LAND COVER SEASONALITY IN SENTINEL-1 TIME SERIES DATA. *ISPRS Annals of the Photogrammetry, Remote Sensing and Spatial Information Sciences*, *V-3–2020*, 97–104. XXIV ISPRS Congress, Commission III (Volume V-3-2020) - 2020 edition. https://doi.org/10.5194/isprs-annals-V-3-2020-97-2020

Dudley, R. W., Hodgkins, G. A., McHale, M. R., Kolian, M. J., & Renard, B. (2017). Trends in snowmelt-related streamflow timing in the conterminous United States. *Journal of Hydrology*, *547*, 208–221. https://doi.org/10.1016/j.jhydrol.2017.01.051

Elias, E., James, D., Heimel, S., Steele, C., Steltzer, H., & Dott, C. (2021). Implications of observed changes in high mountain snow water storage, snowmelt timing and melt window. *Journal of Hydrology: Regional Studies*, *35*, 100799. https://doi.org/10.1016/j.ejrh.2021.100799

El jabiri, Y., Boudhar, A., Htitiou, A., Sproles, E. A., Bousbaa, M., Bouamri, H., & Chehbouni, A. (2024). A method for robust estimation of snow seasonality metrics from landsat and sentinel-2 time series data over Atlas Mountains scale using Google Earth engine. *Geocarto International*, *39*(1). https://doi.org/10.1080/10106049.2024.2313001

Estes, B. L., Knapp, E. E., Skinner, C. N., Miller, J. D., & Preisler, H. K. (2017). Factors influencing fire severity under moderate burning conditions in the Klamath Mountains, northern california, USA. *Ecosphere*, *8*(5). https://doi.org/10.1002/ecs2.1794

Evan, A. T. (2019). A new method to characterize changes in the seasonal cycle of snowpack. *Journal of Applied Meteorology and Climatology*, *58*(1), 131–143. https://doi.org/10.1175/jamc-d-18-0150.1

Fassnacht, S., Dressler, K., & Bales, R. (2003). Snow water equivalent interpolation for the Colorado River Basin from snow telemetry (SNOTEL) data. *Water Resources Research - WATER RESOUR RES*, *39*. https://doi.org/10.1029/2002WR001512

Fassnacht, S. R., Duncan, C. R., Pfohl, A. K. D., Webb, R. W., Derry, J. E., Sanford, W. E., Reimanis, D. C., & Doskocil, L. G. (2022). Drivers of Dust-Enhanced Snowpack Melt-Out and Streamflow Timing. *Hydrology*, *9*(3), Article 3. https://doi.org/10.3390/hydrology9030047

Fassnacht, S. R., Patterson, G. G., Venable, N. B. H., Cherry, M. L., Pfohl, A. K. D., Sanow, J. E., & Tedesche, M. E. (2020). How Do We Define Climate Change? Considering the Temporal Resolution of Niveo-Meteorological Data. *Hydrology*, *7*(3), Article 3. https://doi.org/10.3390/hydrology7030038

Fassnacht, S. R., Venable, N. B. H., McGrath, D., & Patterson, G. G. (2018). Sub-Seasonal Snowpack Trends in the Rocky Mountain National Park Area, Colorado, USA. *Water*, *10*(5), Article 5. https://doi.org/10.3390/w10050562

Feng, T., Huang, C., Huang, G., Shao, D., & Hao, X. (2024). Estimating snow depth based on dual polarimetric radar index from Sentinel-1 GRD data: A case study in the Scandinavian Mountains. *International Journal of Applied Earth Observation and Geoinformation*, *130*, 103873. https://doi.org/10.1016/j.jag.2024.103873

Foster, J. L., Hall, D. K., Chang, A. T. C., & Rango, A. (1984). An overview of passive microwave snow research and results. *Reviews of Geophysics*, *22*(2), 195–208. https://doi.org/10.1029/RG022i002p00195

Foster, J. L., Sun, C., Walker, J. P., Kelly, R., Chang, A., Dong, J., & Powell, H. (2005). Quantifying the uncertainty in passive microwave snow water equivalent observations. *Remote Sensing of Environment*, *94*(2), 187–203. https://doi.org/10.1016/j.rse.2004.09.012

Gafurov, A., & Bárdossy, A. (2009). Cloud removal methodology from Modis snow cover product. *Hydrology and Earth System Sciences*, *13*(7), 1361–1373. https://doi.org/10.5194/hess-13-1361-2009

Gagliano, E., Shean, D., Henderson, S., & Vanderwilt, S. (2023). Capturing the Onset of Mountain Snowmelt Runoff Using Satellite Synthetic Aperture Radar. *Geophysical Research Letters*, *50*(21), e2023GL105303. https://doi.org/10.1029/2023GL105303

Gao, B., & Ma, W. (2024). Capturing snowmelt runoff onset date under different land cover types using synthetic aperture radar: Case Study of Sierra Nevada Mountains, USA. *Applied Sciences*, *14*(15), 6844. https://doi.org/10.3390/app14156844

Gascoin, S., Barrou Dumont, Z., Deschamps-Berger, C., Marti, F., Salgues, G., López-Moreno, J. I., Revuelto, J., Michon, T., Schattan, P., & Hagolle, O. (2020). Estimating Fractional Snow Cover in Open Terrain from Sentinel-2 Using the Normalized Difference Snow Index. *Remote Sensing*, *12*(18), Article 18. https://doi.org/10.3390/rs12182904

Gascoin, S., Grizonnet, M., Bouchet, M., Salgues, G., & Hagolle, O. (2019). Theia Snow collection: High-resolution operational snow cover maps from Sentinel-2 and Landsat-8 data. *Earth System Science Data*, *11*(2), 493–514. https://doi.org/10.5194/essd-11-493-2019

Gascoin, S., Luojus, K., Nagler, T., Lievens, H., Masiokas, M., Jonas, T., Zheng, Z., & De Rosnay, P. (2024). Remote sensing of mountain snow from space: Status and recommendations. *Frontiers in Earth Science*, *12*. https://doi.org/10.3389/feart.2024.1381323

Gascoin, S., Monteiro, D., & Morin, S. (2022). Reanalysis-based contextualization of real-time snow cover monitoring from space. *Environmental Research Letters*, *17*(11), 114044. https://doi.org/10.1088/1748-9326/ac9e6a

Gascon, F., Bouzinac, C., Thépaut, O., Jung, M., Francesconi, B., Louis, J., Lonjou, V., Lafrance, B., Massera, S., Gaudel-Vacaresse, A., Languille, F., Alhammoud, B., Viallefont, F., Pflug, B., Bieniarz, J., Clerc, S., Pessiot, L., Trémas, T., Cadau, E., … Fernandez, V. (2017). Copernicus Sentinel-2A Calibration and Products Validation Status. *Remote Sensing*, *9*(6), Article 6. https://doi.org/10.3390/rs9060584

Gayler, J. M., & Skiles, S. M. (2024). Response of Land Surface Albedo to Fire Disturbance in the Sierra Nevada Seasonal Snow Zone Over the MODIS Record. *Earth's Future*, *12*(6), e2023EF004172. https://doi.org/10.1029/2023EF004172

George G. Ice, Daniel G. Neary, & Paul W. Adams. (2004). Effects of Wildfire on Soils and Watershed Processes. *Journal of Forestry*.

Gerald J. Gottfried, Daniel G. Neary, Malchus B. Baker, Jr, & Peter F. Ffolliott. (n.d.). *Impacts of Wildfires on Hydrologic Processes in Forest Ecosystems: Two Case Studies*. https://corpora.tika.apache.org/base/docs/govdocs1/137/137899.pdf

Gerardo, R., & de Lima, I. P. (2023). Comparing the Capability of Sentinel-2 and Landsat 9 Imagery for Mapping Water and Sandbars in the River Bed of the Lower Tagus River (Portugal). *Remote Sensing*, *15*(7), Article 7. https://doi.org/10.3390/rs15071927

Gersh, M., Gleason, K. E., & Surunis, A. (2022). Forest Fire Effects on Landscape Snow Albedo Recovery and Decay. *Remote Sensing*, *14*(16), Article 16. https://doi.org/10.3390/rs14164079

Giovando, J., & Niemann, J. D. (2022). Wildfire Impacts on Snowpack Phenology in a Changing Climate Within the Western U.S. *Water Resources Research*, *58*(8), e2021WR031569. https://doi.org/10.1029/2021WR031569

Girona-Mata, M., Miles, E. S., Ragettli, S., & Pellicciotti, F. (2019). High-Resolution Snowline Delineation From Landsat Imagery to Infer Snow Cover Controls in a Himalayan Catchment. *Water Resources Research*, *55*(8), 6754–6772. https://doi.org/10.1029/2019WR024935

Gleason, K. E., McConnell, J. R., Arienzo, M. M., Chellman, N., & Calvin, W. M. (2019). Four-fold increase in solar forcing on snow in western U.S. burned forests since 1999. *Nature Communications*, *10*(1), 2026. https://doi.org/10.1038/s41467-019-09935-y

Gleason, K. E., & Nolin, A. W. (2016). Charred forests accelerate snow albedo decay: Parameterizing the post-fire radiative forcing on snow for three years following fire. *Hydrological Processes*, *30*(21), 3855–3870. https://doi.org/10.1002/hyp.10897

Global seasonal Sentinel-1 interferometric coherence and backscatter data set | Scientific Data. (n.d.). Retrieved October 23, 2024, from https://www.nature.com/articles/s41597-022-01189-6

Gong, H., Yu, Z., Zhang, S., & Zhou, G. (2024). Detection of Wet Snow by Weakly Supervised Deep Learning Change Detection Algorithm with Sentinel-1 Data. *Remote Sensing*, *16*(19), Article 19. https://doi.org/10.3390/rs16193575

Hagmann, R. K., Hessburg, P. F., Prichard, S. J., Povak, N. A., Brown, P. M., Fulé, P. Z., Keane, R. E., Knapp, E. E., Lydersen, J. M., Metlen, K. L., Reilly, M. J., Sánchez Meador, A. J., Stephens, S. L., Stevens, J. T., Taylor, A. H., Yocom, L. L., Battaglia, M. A., Churchill, D. J., Daniels, L. D., … Waltz, A. E. (2021). Evidence for widespread changes in the structure, composition, and fire regimes of western North American forests. *Ecological Applications*, *31*(8). https://doi.org/10.1002/eap.2431

Hale, K. E., Jennings, K. S., Musselman, K. N., Livneh, B., & Molotch, N. P. (2023). Recent decreases in snow water storage in western North America. *Communications Earth & Environment*, *4*(1), 1–11. https://doi.org/10.1038/s43247-023-00751-3

Hale, K. E., Musselman, K. N., Newman, A. J., Livneh, B., & Molotch, N. P. (2023). Effects of snow water storage on hydrologic partitioning across the mountainous, western United States. *Water Resources Research*, *59*(8). https://doi.org/10.1029/2023wr034690

Hale, K. E., Musselman, K. N., Bjarke, N. R., Livneh, B., Hinckley, E. S., & Molotch, N. P. (2024). Changes in snow water storage and hydrologic partitioning in an Alpine catchment in the Colorado Front Range. *Hydrological Processes*, *38*(7). https://doi.org/10.1002/hyp.15206

Haleakala, K., Gebremichael, M., Dozier, J., & Lettenmaier, D. P. (2021). *Factors Governing Winter Snow Accumulation and Ablation Susceptibility across the Sierra Nevada (United States)*. https://doi.org/10.1175/JHM-D-20-0257.1

Hall, D. K., Kelly, R. E. J., Riggs, G. A., Chang, A. T. C., & Foster, J. L. (2002). Assessment of the relative accuracy of hemispheric-scale snow-cover maps. *Annals of Glaciology*, *34*, 24–30. https://doi.org/10.3189/172756402781817770

Hall, D. K., Riggs, G. A., DiGirolamo, N. E., & Román, M. O. (2019). Evaluation of MODIS and VIIRS cloud-gap-filled snow-cover products for production of an Earth science data record. *Hydrology and Earth System Sciences*, *23*(12), 5227–5241. https://doi.org/10.5194/hess-23-5227-2019

Hall, D. K., Riggs, G. A., & Salomonson, V. V. (1995). Development of methods for mapping global snow cover using moderate resolution imaging spectroradiometer data. *Remote Sensing of Environment*, *54*(2), 127–140. https://doi.org/10.1016/0034-4257(95)00137-P

Hall, D. K., Sturm, M., Benson, C. S., Chang, A. T. C., Foster, J. L., Garbeil, H., & Chacho, E. (1991). Passive microwave remote and *in situ* measurements of artic and subarctic snow covers in Alaska. *Remote Sensing of Environment*, *38*(3), 161–172. https://doi.org/10.1016/0034-4257(91)90086-L

Hallema, D. W., Sun, G., Caldwell, P. V., Norman, S. P., Cohen, E. C., Liu, Y., Bladon, K. D., & McNulty, S. G. (2018). Burned forests impact water supplies. *Nature Communications*, *9*(1). https://doi.org/10.1038/s41467-018-03735-6

Hallikainen, M. T., Halme, P., Takala, M., & Pulliainen, J. (2003). Combined active and passive microwave remote sensing of snow in Finland. *IGARSS 2003. 2003 IEEE International Geoscience and Remote Sensing Symposium. Proceedings (IEEE Cat. No.03CH37477)*, *2*, 830–832 vol.2. https://doi.org/10.1109/IGARSS.2003.1293934

Hammond, J. C., Saavedra, F. A., & Kampf, S. K. (2018a). Global snow zone maps and trends in snow persistence 2001–2016. *International Journal of Climatology*, *38*(12), 4369–4383. https://doi.org/10.1002/joc.5674

Hammond, J. C., Saavedra, F. A., & Kampf, S. K. (2018b). How Does Snow Persistence Relate to Annual Streamflow in Mountain Watersheds of the Western U.S. With Wet Maritime and Dry Continental Climates? *Water Resources Research*, *54*(4), 2605–2623. https://doi.org/10.1002/2017WR021899

Harpold, A. A., Biederman, J. A., Condon, K., Merino, M., Korgaonkar, Y., Nan, T., Sloat, L. L., Ross, M., & Brooks, P. D. (2013). Changes in snow accumulation and ablation following the Las Conchas forest fire, New Mexico, USA. *Ecohydrology*, *7*(2), 440–452. https://doi.org/10.1002/eco.1363

Harrison, H. N., Hammond, J. C., Kampf, S., & Kiewiet, L. (2021). On the hydrological difference between catchments above and below the intermittent-persistent snow transition. *Hydrological Processes*, *35*(11). https://doi.org/10.1002/hyp.14411

Hatchett, B. J., Rhoades, A. M., & McEvoy, D. J. (2022). Decline in Seasonal Snow during a Projected 20-Year Dry Spell. *Hydrology*, *9*(9), Article 9. https://doi.org/10.3390/hydrology9090155

Heidari, H., Arabi, M., & Warziniack, T. (2021). Vulnerability to water shortage under current and future water supply-demand conditions across U.S. river basins. *Earth's Future*, *9*(10). https://doi.org/10.1029/2021ef002278

Heidari, H., Arabi, M., Warziniack, T., & Sharvelle, S. (2021). Effects of urban development patterns on municipal water shortage. *Frontiers in Water*, *3*. https://doi.org/10.3389/frwa.2021.694817

Higuera, P. E., Shuman, B. N., & Wolf, K. D. (2021). Rocky Mountain subalpine forests now burning more than any time in recent millennia. *Proceedings of the National Academy of Sciences*, *118*(25). https://doi.org/10.1073/pnas.2103135118

Heldmyer, A., Livneh, B., Molotch, N., & Rajagopalan, B. (2021). Investigating the Relationship Between Peak Snow-Water Equivalent and Snow Timing Indices in the Western United States and Alaska. *Water Resources Research*, *57*(5), e2020WR029395. https://doi.org/10.1029/2020WR029395

Herbert, J. N., Raleigh, M. S., & Small, E. E. (2024). Reanalyzing the spatial representativeness of snow depth at automated monitoring stations using airborne lidar data. *The Cryosphere*, *18*(8), 3495–3512. https://doi.org/10.5194/tc-18-3495-2024

HESS - Canopy structure, topography, and weather are equally important drivers of small-scale snow cover dynamics in sub-alpine forests. (n.d.). Retrieved September 16, 2024, from https://hess.copernicus.org/articles/27/2099/2023/hess-27-2099-2023.html

HESS - Evaluation of MODIS and VIIRS cloud-gap-filled snow-cover products for production of an Earth science data record. (n.d.). Retrieved September 5, 2024, from https://hess.copernicus.org/articles/23/5227/2019/

Hofmeister, F., Arias-Rodriguez, L. F., Premier, V., Marin, C., Notarnicola, C., Disse, M., & Chiogna, G. (2022). Intercomparison of Sentinel-2 and modelled snow cover maps in a high-elevation Alpine catchment. *Journal of Hydrology X*, *15*, 100123. https://doi.org/10.1016/j.hydroa.2022.100123

Hohner, A. K., Rhoades, C. C., Wilkerson, P., & Rosario-Ortiz, F. L. (2019). Wildfires Alter Forest Watersheds and Threaten Drinking Water Quality. *Accounts of Chemical Research*, *52*(5), 1234–1244. https://doi.org/10.1021/acs.accounts.8b00670

Hoppinen, Z., Palomaki, R. T., Brencher, G., Dunmire, D., Gagliano, E., Marziliano, A., Tarricone, J., & Marshall, H.-P. (2024). Evaluating snow depth retrievals from sentinel-1 volume scattering over NASA snowex sites. *The Cryosphere*, *18*(11), 5407–5430. https://doi.org/10.5194/tc-18-5407-2024

Hydrological Processes | Hydrology Journal | Wiley Online Library. (n.d.). Retrieved February 1, 2024, from https://onlinelibrary.wiley.com/doi/10.1002/hyp.7128

Ice, G. G., Neary, D. G., & Adams, P. W. (2004). Effects of Wildfire on Soils and Watershed Processes. *Journal of Forestry*, *102*(6), 16–20. https://doi.org/10.1093/jof/102.6.16

Interpreting Sentinel-1 SAR Backscatter Signals of Snowpack Surface Melt/Freeze, Warming, and Ripening, through Field Measurements and Physically-Based SnowModel. (n.d.). Retrieved October 23, 2024, from https://www.mdpi.com/2072-4292/14/16/4002

Jacob, A. W., Vicente-Guijalba, F., Lopez-Martinez, C., Lopez-Sanchez, J. M., Litzinger, M., Kristen, H., Mestre-Quereda, A., Ziółkowski, D., Lavalle, M., Notarnicola, C., Suresh, G., Antropov, O., Ge, S., Praks, J., Ban, Y., Pottier, E., Mallorquí Franquet, J. J., Duro, J., & Engdahl, M. E. (2020). Sentinel-1 InSAR Coherence for Land Cover Mapping: A Comparison of Multiple Feature-Based Classifiers. *IEEE Journal of Selected Topics in Applied Earth Observations and Remote Sensing*, *13*, 535–552. IEEE Journal of Selected Topics in Applied Earth Observations and Remote Sensing. https://doi.org/10.1109/JSTARS.2019.2958847

Jepsen, S. M., Molotch, N. P., Williams, M. W., Rittger, K. E., & Sickman, J. O. (2012). Interannual variability of snowmelt in the Sierra Nevada and Rocky Mountains, United States: Examples from two alpine watersheds. *Water Resources Research*, *48*(2). https://doi.org/10.1029/2011WR011006

Jia, Y., Lund, R., Kong, J., Dyer, J., Woody, J., & Marron, J. S. (2023). Trends in Northern Hemispheric Snow Presence. *Journal of Hydrometeorology*, *24*(6), 1137–1154. https://doi.org/10.1175/JHM-D-22-0182.1

Justice, C. O., Vermote, E., Townshend, J. R. G., Defries, R., Roy, D. P., Hall, D. K., Salomonson, V. V., Privette, J. L., Riggs, G., Strahler, A., Lucht, W., Myneni, R. B., Knyazikhin, Y., Running, S. W., Nemani, R. R., Zhengming Wan, Huete, A. R., van Leeuwen, W., Wolfe, R. E., … Barnsley, M. J. (1998). The moderate resolution imaging Spectroradiometer (MODIS): Land Remote Sensing for Global Change Research. *IEEE Transactions on Geoscience and Remote Sensing*, *36*(4), 1228–1249. https://doi.org/10.1109/36.701075

Kampf, S. K., McGrath, D., Sears, M. G., Fassnacht, S. R., Kiewiet, L., & Hammond, J. C. (2022). Increasing wildfire impacts on snowpack in the western U.S. *Proceedings of the National Academy of Sciences*, *119*(39), e2200333119. https://doi.org/10.1073/pnas.2200333119

Kane, V. R., Cansler, C. A., Povak, N. A., Kane, J. T., McGaughey, R. J., Lutz, J. A., Churchill, D. J., & North, M. P. (2015). Mixed severity fire effects within the rim fire: Relative importance of local climate, fire weather, topography, and forest structure. *Forest Ecology and Management*, *358*, 62–79. https://doi.org/10.1016/j.foreco.2015.09.001

Karbou, F., Veyssière, G., Coleou, C., Dufour, A., Gouttevin, I., Durand, P., Gascoin, S., & Grizonnet, M. (2021). Monitoring Wet Snow Over an Alpine Region Using Sentinel-1 Observations. *Remote Sensing*, *13*(3), Article 3. https://doi.org/10.3390/rs13030381

Keane, R. E., Rollins, M., & Zhu, Z.-L. (2007). Using simulated historical time series to prioritize fuel treatments on landscapes across the United States: The LANDFIRE prototype project. *Ecological Modelling*, *204*(3), 485–502. https://doi.org/10.1016/j.ecolmodel.2007.02.005

Kellndorfer, J., Cartus, O., Lavalle, M., Magnard, C., Milillo, P., Oveisgharan, S., Osmanoglu, B., Rosen, P. A., & Wegmüller, U. (2022). Global seasonal Sentinel-1 interferometric coherence and backscatter data set. *Scientific Data*, *9*(1), Article 1. https://doi.org/10.1038/s41597-022-01189-6

Kelly E. Gleason. (n.d.). *Charred forests increase snowmelt: Effects of burned woody debris and incoming solar radiation on snow ablation—Gleason—2013—Geophysical Research Letters—Wiley Online Library*. Retrieved September 4, 2024, from https://agupubs.onlinelibrary.wiley.com/doi/10.1002/grl.50896

Keskinen, Z., & Marshall, H.-P. (2022). *Using InSAR in Snow—Uavsar Coherence in the SnowEx Campaigns*. *2022*, C22E-0811. AGU Fall Meeting Abstracts.

Keyser, A., & Westerling, A. L. (2017). Climate drives inter-annual variability in probability of high severity fire occurrence in the western United States. *Environmental Research Letters*, *12*(6), 065003. https://doi.org/10.1088/1748-9326/aa6b10

Klein, A. G., & Barnett, A. C. (2003). Validation of daily MODIS snow cover maps of the Upper Rio Grande River Basin for the 2000–2001 snow year. *Remote Sensing of Environment*, *86*(2), 162–176. https://doi.org/10.1016/S0034-4257(03)00097-X

Kollert, A., Mayr, A., Dullinger, S., Hülber, K., Moser, D., Lhermitte, S., Gascoin, S., & Rutzinger, M. (2024). Downscaling MODIS NDSI to Sentinel-2 fractional snow cover by random forest regression. *Remote Sensing Letters*, *15*(4), 363–372. https://doi.org/10.1080/2150704X.2024.2327084

Kongoli, C., Dean, C. A., Helfrich, S. R., & Ferraro, R. R. (2007). Evaluating the potential of a blended passive microwave-interactive multi-sensor product for improved mapping of snow cover and estimations of snow water equivalent. *Hydrological Processes*, *21*(12), 1597–1607. https://doi.org/10.1002/hyp.6722

Koshkin, A. L., Hatchett, B. J., & Nolin, A. W. (2022). Wildfire impacts on western United States snowpacks. *Frontiers in Water*, *4*. https://doi.org/10.3389/frwa.2022.971271

Kreider, M. R., Higuera, P. E., Parks, S. A., Rice, W. L., White, N., & Larson, A. J. (2024). Fire suppression makes wildfires more severe and accentuates impacts of climate change and fuel accumulation. *Nature Communications*, *15*(1). https://doi.org/10.1038/s41467-024-46702-0

Lead-lag correlations between snow cover and meteorological factors at multi-time scales in the Tibetan Plateau under climate warming | Theoretical and Applied Climatology. (n.d.). Retrieved September 5, 2024, from https://link.springer.com/article/10.1007/s00704-021-03802-x

Leopardi, M., & Scorzini, A. R. (2015). Effects of wildfires on peak discharges in watersheds. *iForest - Biogeosciences and Forestry*, *8*(3), 302. https://doi.org/10.3832/ifor1120-007

Li, D., Durand, M., & Margulis, S. A. (2012). Potential for hydrologic characterization of Deep Mountain snowpack via passive microwave remote sensing in the Kern River Basin, Sierra Nevada, USA. *Remote Sensing of Environment*, *125*, 34–48. https://doi.org/10.1016/j.rse.2012.06.027

Li, D., Wrzesien, M. L., Durand, M., Adam, J., & Lettenmaier, D. P. (2017). How much runoff originates as snow in the western United States, and how will that change in the future? *Geophysical Research Letters*, *44*(12), 6163–6172. https://doi.org/10.1002/2017gl073551

Li, H., Wang, Z., He, G., & Man, W. (2017). Estimating Snow Depth and Snow Water Equivalence Using Repeat-Pass Interferometric SAR in the Northern Piedmont Region of the Tianshan Mountains. *Journal of Sensors*, *2017*, e8739598. https://doi.org/10.1155/2017/8739598

Liang, D., Guo, H., Zhang, L., Cheng, Y., Zhu, Q., & Liu, X. (2021). Time-series snowmelt detection over the Antarctic using Sentinel-1 SAR images on Google Earth Engine. *Remote Sensing of Environment*, *256*, 112318. https://doi.org/10.1016/j.rse.2021.112318

Lievens, H., Brangers, I., Marshall, H.-P., Jonas, T., Olefs, M., & De Lannoy, G. (2022). Sentinel-1 snow depth retrieval at sub-kilometer resolution over the European Alps. *The Cryosphere*, *16*(1), 159–177. https://doi.org/10.5194/tc-16-159-2022

Littell, J. S., McKenzie, D., Peterson, D. L., & Westerling, A. L. (2009). Climate and wildfire area burned in western U.S. ecoprovinces, 1916–2003. *Ecological Applications*, *19*(4), 1003–1021. https://doi.org/10.1890/07-1183.1

Liu, Y., Chen, X., Hao, J.-S., & Li, L. (2020). Snow cover estimation from MODIS and Sentinel-1 SAR data using machine learning algorithms in the western part of the Tianshan Mountains. *Journal of Mountain Science*, *17*(4), 884–897. https://doi.org/10.1007/s11629-019-5723-1

Livneh, B., & Badger, A. M. (2020). Drought less predictable under declining future snowpack. *Nature Climate Change*, *10*(5), Article 5. https://doi.org/10.1038/s41558-020-0754-8

Lund, J., Forster, R. R., Deeb, E. J., Liston, G. E., Skiles, S. M., & Marshall, H.-P. (2022). Interpreting Sentinel-1 SAR Backscatter Signals of Snowpack Surface Melt/Freeze, Warming, and Ripening, through Field Measurements and Physically-Based SnowModel. *Remote Sensing*, *14*(16), Article 16. https://doi.org/10.3390/rs14164002

Lund, J., Forster, R. R., Rupper, S. B., Deeb, E. J., Marshall, H. P., Hashmi, M. Z., & Burgess, E. (2020). Mapping Snowmelt Progression in the Upper Indus Basin With Synthetic Aperture Radar. *Frontiers in Earth Science*, *7*. https://www.frontiersin.org/articles/10.3389/feart.2019.00318

Lundquist, J. D., Dickerson-Lange, S. E., Lutz, J. A., & Cristea, N. C. (2013). Lower Forest density enhances snow retention in regions with warmer winters: A global framework developed from plot-scale observations and modeling. *Water Resources Research*, *49*(10), 6356–6370. https://doi.org/10.1002/wrcr.20504

Luojus, K. P., Pulliainen, J. T., Metsamaki, S. J., & Hallikainen, M. T. (2006). Accuracy assessment of SAR data-based snow-covered area estimation method. *IEEE Transactions on Geoscience and Remote Sensing*, *44*(2), 277–287. https://doi.org/10.1109/tgrs.2005.861414

Mahmoodzada, A. B., Das, P., Varade, D., Akhtar, M. A., & Shimada, S. (2024). High-resolution mapping of seasonal snow cover extent in the Pamir Hindu Kush using machine learning-based integration of multi-sensor data. *Acta Geophysica*, *72*(2), 1455–1470. https://doi.org/10.1007/s11600-023-01281-4

Mahmoodzada, A. B., Varade, D., Shimada, S., Rezazada, F. A., Mahmoodzada, A. S., Jawher, A. N., & Toghyan, M. (2022). Capability assessment of Sentinel-1 data for estimation of snow hydrological potential in the Khanabad watershed in the Hindu Kush Himalayas of Afghanistan. *Remote Sensing Applications: Society and Environment*, *26*, 100758. https://doi.org/10.1016/j.rsase.2022.100758

Mankin, J. S., Viviroli, D., Singh, D., Hoekstra, A. Y., & Diffenbaugh, N. S. (2015). The potential for snow to supply human water demand in the present and future. *Environmental Research Letters*, *10*(11), 114016. https://doi.org/10.1088/1748-9326/10/11/114016

Mapping Radar Glacier Zones and Dry Snow Line in the Antarctic Peninsula Using Sentinel-1 Images. (n.d.). Retrieved October 23, 2024, from https://www.mdpi.com/2072-4292/9/11/1171

Marin, C., Bertoldi, G., Premier, V., Callegari, M., Brida, C., Hürkamp, K., Tschiersch, J., Zebisch, M., & Notarnicola, C. (2020). Use of Sentinel-1 radar observations to evaluate snowmelt dynamics in alpine regions. *The Cryosphere*, *14*(3), 935–956. https://doi.org/10.5194/tc-14-935-2020

Markus, T., Powell, D. C., & Wang, J. R. (2006). Sensitivity of passive microwave snow depth retrievals to weather effects and snow evolution. *IEEE Transactions on Geoscience and Remote Sensing*, *44*(1), 68–77. IEEE Transactions on Geoscience and Remote Sensing. https://doi.org/10.1109/TGRS.2005.860208

Marlon, J. R., Bartlein, P. J., Gavin, D. G., Long, C. J., Anderson, R. S., Briles, C. E., Brown, K. J., Colombaroli, D., Hallett, D. J., Power, M. J., Scharf, E. A., & Walsh, M. K. (2012). Long-term perspective on wildfires in the western USA. *Proceedings of the National Academy of Sciences*, *109*(9), E535–E543. https://doi.org/10.1073/pnas.1112839109

Massart, S., Vreugdenhil, M., Bauer-Marschallinger, B., Navacchi, C., Raml, B., & Wagner, W. (2024). Mitigating the impact of dense vegetation on the Sentinel-1 surface soil moisture retrievals over Europe. *European Journal of Remote Sensing*, *57*(1), 2300985. https://doi.org/10.1080/22797254.2023.2300985

Masson, T., Dumont, M., Mura, M. D., Sirguey, P., Gascoin, S., Dedieu, J.-P., & Chanussot, J. (2018). An Assessment of Existing Methodologies to Retrieve Snow Cover Fraction from MODIS Data. *Remote Sensing*, *10*(4), Article 4. https://doi.org/10.3390/rs10040619

Maxwell, J. D., Call, A., & St. Clair, S. B. (2019). Wildfire and topography impacts on snow accumulation and retention in montane forests. *Forest Ecology and Management*, *432*, 256–263. https://doi.org/10.1016/j.foreco.2018.09.021

Mazzotti, G., Webster, C., Quéno, L., Cluzet, B., & Jonas, T. (2023). Canopy structure, topography, and weather are equally important drivers of small-scale snow cover dynamics in sub-alpine forests. *Hydrology and Earth System Sciences*, *27*(11), 2099–2121. https://doi.org/10.5194/hess-27-2099-2023

McCullough, I. M., Loftin, C., & Sader, S. A. (2013, January). Comparison of Landsat and modis specifications | download table. https://www.researchgate.net/figure/Comparison-of-Landsat-and-MODIS-specifications_tbl1_304124818

McDonald, R. I., Green, P., Balk, D., Fekete, B. M., Revenga, C., Todd, M., & Montgomery, M. (2011). Urban growth, climate change, and freshwater availability. *Proceedings of the National Academy of Sciences*, *108*(15), 6312–6317. https://doi.org/10.1073/pnas.1011615108

McGrath, D., Zeller, L., Bonnell, R., Reis, W., Kampf, S., Williams, K., Okal, M., Olsen-Mikitowicz, A., Bump, E., Sears, M., & Rittger, K. (2023). Declines in Peak Snow Water Equivalent and Elevated Snowmelt Rates Following the 2020 Cameron Peak Wildfire in Northern Colorado. *Geophysical Research Letters*, *50*(6), e2022GL101294. https://doi.org/10.1029/2022GL101294

Meromy, L., Molotch, N. P., Link, T. E., Fassnacht, S. R., & Rice, R. (2013). Subgrid variability of snow water equivalent at operational snow stations in the western USA. *Hydrological Processes*, *27*(17), 2383–2400. https://doi.org/10.1002/hyp.9355

Microsoft. (n.d.). *Microsoft Planetary Computer Sentinel 1 Radiometrically Terrain Corrected (RTC)*. Retrieved September 4, 2024, from https://planetarycomputer.microsoft.com/dataset/sentinel-1-rtc#Example-Notebook

Miller, J. D., Safford, H. D., Crimmins, M., & Thode, A. E. (2009). Quantitative Evidence for Increasing Forest Fire Severity in the Sierra Nevada and Southern Cascade Mountains, California and Nevada, USA. *Ecosystems*, *12*(1), 16–32. https://doi.org/10.1007/s10021-008-9201-9

Mohammad M. Hasan, Steven J. Burian & Michael E. Barber. (n.d.). *Determining The Impacts Of Wildfires On Peak Flood Flows In High Mountain Watersheds*. Retrieved September 4, 2024, from https://www.witpress.com/elibrary/ei-volumes/3/4/2729

Molotch, N. P., Fassnacht, S. R., Bales, R. C., & Helfrich, S. R. (2004). Estimating the distribution of snow water equivalent and snow extent beneath cloud cover in the Salt–Verde River basin, Arizona. *Hydrological Processes*, *18*(9), 1595–1611. https://doi.org/10.1002/hyp.1408

Moore, C., Kampf, S., Stone, B., & Richer, E. (2014). A GIS-based method for defining snow zones: Application to the western united states. *Geocarto International*, *30*(1), 62–81. https://doi.org/10.1080/10106049.2014.885089

Mote, P. W., Hamlet, A. F., Clark, M. P., & Lettenmaier, D. P. (2005). Declining mountain snowpack in western North America*. *Bulletin of the American Meteorological Society*, *86*(1), 39–50. https://doi.org/10.1175/bams-86-1-39

Nagajothi V., Priya M. Geetha, & Sharma Parmand. (2019). Https://www.indianjournals.com/ijor.aspx?target=ijor:ije1&volume=46&issue=1&article=016. *Indian Journal of Ecology*, *46*(1). https://www.indianjournals.com/ijor.aspx?target=ijor:ije1&volume=46&issue=1&article=016

Nagler, T., Rott, H., Bippus, G., & Ripper, E. (2013). *Preparation for Snow Cover Monitoring Using Sentinel-1 and Sentinel-3 Data*. EGU2013-6275. EGU General Assembly Conference Abstracts.

Nagler, T., Rott, H., Ripper, E., Bippus, G., & Hetzenecker, M. (2016). Advancements for snowmelt monitoring by means of sentinel-1 sar. *Remote Sensing*, *8*(4), 348. https://doi.org/10.3390/rs8040348

Neary, D. G., Gottfried, G. J., DeBano, L. F., & Tecle, A. (2003). Impacts of Fire on Watershed Resources. *Journal of the Arizona-Nevada Academy of Science*, *35*(1), 23–41.

NLCD 2021 USFS Tree Canopy Cover (CONUS) | Multi-Resolution Land Characteristics (MRLC) Consortium. (n.d.). Retrieved September 4, 2024, from https://www.mrlc.gov/data/nlcd-2021-usfs-tree-canopy-cover-conus

Notarnicola, C., Ratti, R., Maddalena, V., Schellenberger, T., Ventura, B., & Zebisch, M. (2013). Seasonal Snow Cover Mapping in Alpine Areas Through Time Series of COSMO-SkyMed Images. *IEEE Geoscience and Remote Sensing Letters*, *10*(4), 716–720. IEEE Geoscience and Remote Sensing Letters. https://doi.org/10.1109/LGRS.2012.2219848

Parajka, J., & Blöschl, G. (2006). Validation of modis snow cover images over Austria. *Hydrology and Earth System Sciences*, *10*(5), 679–689. https://doi.org/10.5194/hess-10-679-2006

Parajka, J., & Blöschl, G. (2008). Spatio-temporal combination of MODIS images – potential for snow cover mapping. *Water Resources Research*, *44*(3). https://doi.org/10.1029/2007WR006204

Parks, S. A., Holsinger, L. M., Blankenship, K., Dillon, G. K., Goeking, S. A., & Swaty, R. (2023). Contemporary wildfires are more severe compared to the historical reference period in western US dry conifer forests. *Forest Ecology and Management*, *544*, 121232. https://doi.org/10.1016/j.foreco.2023.121232

Paul V. Dunnette, Philip E. Higuera, Kendra K. McLauchlan, Kelly M. Derr, Christy E. Briles, Margaret H. Keefe. (n.d.). *Biogeochemical impacts of wildfires over four millennia in a Rocky Mountain subalpine watershed—Dunnette—2014—New Phytologist—Wiley Online Library*. Retrieved September 4, 2024, from https://nph.onlinelibrary.wiley.com/doi/full/10.1111/nph.12828

(PDF) Snow monitoring in midlatitude lowlands using SAR backscattering ratio. (n.d.). Retrieved October 23, 2024, from https://www.researchgate.net/publication/360205960_Snow_monitoring_in_midlatitude_lowlands_using_SAR_backscattering_ratio

Penn, C. A., Clow, D. W., Sexstone, G. A., & Murphy, S. F. (2020). Changes in Climate and Land Cover Affect Seasonal Streamflow Forecasts in the Rio Grande Headwaters. *JAWRA Journal of the American Water Resources Association*, *56*(5), 882–902. https://doi.org/10.1111/1752-1688.12863

Povak, N. A., Hessburg, P. F., & Salter, R. B. (2018). Evidence for scale-dependent topographic controls on wildfire spread. *Ecosphere*, *9*(10). https://doi.org/10.1002/ecs2.2443

Pu, Z., Xu, L., & Salomonson, V. V. (2007). Modis/Terra observed seasonal variations of snow cover over the Tibetan Plateau. *Geophysical Research Letters*, *34*(6). https://doi.org/10.1029/2007gl029262

Qiao, X., Liu, J., Wang, S., Wang, J., Ji, H., Chen, X., Liu, H., & Lu, F. (2021). Lead-lag correlations between snow cover and meteorological factors at multi-time scales in the Tibetan Plateau under climate warming. *Theoretical and Applied Climatology*, *146*(3), 1459–1477. https://doi.org/10.1007/s00704-021-03802-x

Ramage, J. M., McKenney, R. A., Thorson, B., Maltais, P., & Kopczynski, S. E. (2006). Relationship between passive microwave-derived snowmelt and surface-measured discharge, Wheaton River, Yukon Territory, Canada. *HYDROLOGICAL PROCESSES*, *20*(4), 689–704. 62nd Eastern Snow Conference (ESC). https://doi.org/10.1002/hyp.6133

Reanalysis-based contextualization of real-time snow cover monitoring from space—IOPscience. (n.d.). Retrieved October 2, 2024, from https://iopscience.iop.org/article/10.1088/1748-9326/ac9e6a

Revuelto, J., Alonso-González, E., Gascoin, S., Rodríguez-López, G., & López-Moreno, J. I. (2021). Spatial Downscaling of MODIS Snow Cover Observations Using Sentinel-2 Snow Products. *Remote Sensing*, *13*(22), Article 22. https://doi.org/10.3390/rs13224513

Rhoades, C. C., Chow, A. T., Covino, T. P., Fegel, T. S., Pierson, D. N., & Rhea, A. E. (2018). The legacy of a severe wildfire on stream nitrogen and carbon in headwater catchments. *Ecosystems*, *22*(3), 643–657. https://doi.org/10.1007/s10021-018-0293-6

Richer, E. E., Kampf, S. K., Fassnacht, S. R., & Moore, C. C. (2013). Spatiotemporal index for analyzing controls on snow climatology: Application in the Colorado Front Range. *Physical Geography*, *34*(2), 85–107. https://doi.org/10.1080/02723646.2013.787578

Richiardi, C., Siniscalco, C., & Adamo, M. (2023). Comparison of Three Different Random Forest Approaches to Retrieve Daily High-Resolution Snow Cover Maps from MODIS and Sentinel-2 in a Mountain Area, Gran Paradiso National Park (NW Alps). *Remote Sensing*, *15*(2), Article 2. https://doi.org/10.3390/rs15020343

Robinne, F., Hallema, D. W., Bladon, K. D., Flannigan, M. D., Boisramé, G., Bréthaut, C. M., Doerr, S. H., Di Baldassarre, G., Gallagher, L. A., Hohner, A. K., Khan, S. J., Kinoshita, A. M., Mordecai, R., Nunes, J. P., Nyman, P., Santín, C., Sheridan, G., Stoof, C. R., Thompson, M. P., … Wei, Y. (2021). Scientists' warning on extreme wildfire risks to water supply. *Hydrological Processes*, *35*(5). https://doi.org/10.1002/hyp.14086

Robinne, F.-N., Hallema, D. W., Bladon, K. D., & Buttle, J. M. (2020). Wildfire impacts on Hydrologic Ecosystem Services in North American high-latitude forests: A scoping review. *Journal of Hydrology*, *581*, 124360. https://doi.org/10.1016/j.jhydrol.2019.124360

Romanov, P., Gutman, G., & Csiszar, I. (2000). *Automated Monitoring of Snow Cover over North America with Multispectral Satellite Data*. https://journals.ametsoc.org/view/journals/apme/39/11/1520-0450_2000_039_1866_amosco_2.0.co_2.xml

Rosenthal, W., & Dozier, J. (1996). Automated Mapping of Montane Snow Cover at Subpixel Resolution from the Landsat Thematic Mapper. *Water Resources Research*, *32*(1), 115–130. https://doi.org/10.1029/95WR02718

Roy, D. P., Wulder, M. A., Loveland, T. R., C.E., W., Allen, R. G., Anderson, M. C., Helder, D., Irons, J. R., Johnson, D. M., Kennedy, R., Scambos, T. A., Schaaf, C. B., Schott, J. R., Sheng, Y., Vermote, E. F., Belward, A. S., Bindschadler, R., Cohen, W. B., Gao, F., … Zhu, Z. (2014). Landsat-8: Science and product vision for terrestrial global change research. *Remote Sensing of Environment*, *145*, 154–172. https://doi.org/10.1016/j.rse.2014.02.001

Rumsey, C. A., Miller, M. P., & Sexstone, G. A. (2020). Relating hydroclimatic change to streamflow, baseflow, and hydrologic partitioning in the Upper Rio Grande Basin, 1980 to 2015. *Journal of Hydrology*, *584*, 124715. https://doi.org/10.1016/j.jhydrol.2020.124715

Rutter, N., Essery, R., Baxter, R., Hancock, S., Horton, M., Huntley, B., Reid, T., & Woodward, J. (2023). Canopy structure and air temperature inversions impact simulation of sub-canopy longwave radiation in snow-covered boreal forests. *Journal of Geophysical Research: Atmospheres*, *128*(14). https://doi.org/10.1029/2022jd037980

Saavedra, F. A., Kampf, S. K., Fassnacht, S. R., & Sibold, J. S. (2016). A snow climatology of the Andes mountains from MODIS snow cover data. *International Journal of Climatology*, *37*(3), 1526–1539. https://doi.org/10.1002/joc.4795

Salcedo, A. P., & Cogliati, M. G. (2014). Snow Cover Area Estimation Using Radar and Optical Satellite Information. *Atmospheric and Climate Sciences*, *4*(4), Article 4. https://doi.org/10.4236/acs.2014.44047

Saxe, S., Hogue, T. S., & Hay, L. (2018). Characterization and evaluation of controls on post-fire streamflow response across western US watersheds. *Hydrology and Earth System Sciences*, *22*(2), 1221–1237. https://doi.org/10.5194/hess-22-1221-2018

Seibert, J., McDonnell, J. J., & Woodsmith, R. D. (2010). Effects of wildfire on catchment runoff response: A modelling approach to detect changes in snow-dominated forested catchments. *Hydrology Research*, *41*(5), 378–390. https://doi.org/10.2166/nh.2010.036

Sexstone, G. A., Penn, C. A., Liston, G. E., Gleason, K. E., Moeser, C. D., & Clow, D. W. (2020). Spatial Variability in Seasonal Snowpack Trends across the Rio Grande Headwaters (1984–2017). *Journal of Hydrometeorology*, *21*(11), 2713–2733. https://doi.org/10.1175/JHM-D-20-0077.1

Shen, X., Wang, D., Mao, K., Anagnostou, E., & Hong, Y. (2019). Inundation Extent Mapping by Synthetic Aperture Radar: A Review. *Remote Sensing*, *11*(7), Article 7. https://doi.org/10.3390/rs11070879

Sherriff, R. L., & Veblen, T. T. (2007). A spatially-explicit reconstruction of historical fire occurrence in the Ponderosa Pine Zone of the Colorado Front Range. *Ecosystems*, *10*(2), 311–323. https://doi.org/10.1007/s10021-007-9022-2

Siirila-Woodburn, E. R., Rhoades, A. M., Hatchett, B. J., Huning, L. S., Szinai, J., Tague, C., Nico, P. S., Feldman, D. R., Jones, A. D., Collins, W. D., & Kaatz, L. (2021). A low-to-no snow future and its impacts on water resources in the Western United States. *Nature Reviews Earth & Environment*, *2*(11), 800–819. https://doi.org/10.1038/s43017-021-00219-y

Sibold, J. S., Veblen, T. T., & González, M. E. (2006). Spatial and temporal variation in historic fire regimes in subalpine forests across the Colorado Front Range in Rocky Mountain National Park, Colorado, USA. *Journal of Biogeography*, *33*(4), 631–647. https://doi.org/10.1111/j.1365-2699.2005.01404.x

Simon Planzer. (n.d.). *Estimating Snow Extent From Sentinel-2 Imagery*. Retrieved September 4, 2024, from https://www.simonplanzer.com/articles/cog-ndsi/

Singh, M. K., & Bharti, R. (2023). Inversion model for snow geophysical parameters estimation using sentinel–1 stokes parameter. *Earth Science Informatics*, *16*(2), 1585–1595. https://doi.org/10.1007/s12145-023-00984-y

Snehmani, Singh, M. K., Gupta, R. D., Bhardwaj, A., & Joshi, P. K. (2015). Remote sensing of mountain snow using active microwave sensors: A review. *Geocarto International*, *30*(1), 1–27. https://doi.org/10.1080/10106049.2014.883434

Snow Cover Area Estimation Using Radar and Optical Satellite Information. (n.d.). Retrieved October 23, 2024, from https://www.scirp.org/journal/paperinformation?paperid=49521

Snow Water Equivalent Retrieval Using Active and Passive Microwave Observations—Zhu—2021—Water Resources Research—Wiley Online Library. (n.d.). Retrieved September 4, 2024, from https://agupubs.onlinelibrary.wiley.com/doi/full/10.1029/2020WR027563

Snapir, B., Momblanch, A., Jain, S. K., Waine, T. W., & Holman, I. P. (2019). A method for monthly mapping of wet and dry snow using sentinel-1 and Modis: Application to a Himalayan River Basin. *International Journal of Applied Earth Observation and Geoinformation*, *74*, 222–230. https://doi.org/10.1016/j.jag.2018.09.011

Sokol, J., Pultz, T. J., & Walker, A. E. (2003). Passive and active airborne microwave remote sensing of snow cover. *International Journal of Remote Sensing*, *24*(24), 5327–2344. https://doi.org/10.1080/0143116031000115076

Song, X.-P., Huang, W., Hansen, M. C., & Potapov, P. (2021). An evaluation of Landsat, Sentinel-2, Sentinel-1 and MODIS data for crop type mapping. *Science of Remote Sensing*, *3*, 100018. https://doi.org/10.1016/j.srs.2021.100018

Spatio-temporal combination of MODIS images – potential for snow cover mapping—Parajka—2008—Water Resources Research—Wiley Online Library. (n.d.). Retrieved October 3, 2024, from https://agupubs.onlinelibrary.wiley.com/doi/10.1029/2007WR006204

Spectral signature of alpine snow cover from the landsat thematic mapper—ScienceDirect. (n.d.). Retrieved October 3, 2024, from https://www.sciencedirect.com/science/article/pii/0034425789901016?via%3Dihub

Steel, Z. L., Koontz, M. J., & Safford, H. D. (2018). The changing landscape of wildfire: Burn pattern trends and implications for California's yellow pine and mixed conifer forests. *Landscape Ecology*, *33*(7), 1159–1176. https://doi.org/10.1007/s10980-018-0665-5

Stevens, J. T. (2017). Scale-dependent effects of post-fire canopy cover on snowpack depth in montane coniferous forests. *Ecological Applications*, *27*(6), 1888–1900. https://doi.org/10.1002/eap.1575

Stevens-Rumann, C. S., Kemp, K. B., Higuera, P. E., Harvey, B. J., Rother, M. T., Donato, D. C., Morgan, P., & Veblen, T. T. (2017). Evidence for declining forest resilience to wildfires under climate change. *Ecology Letters*, *21*(2), 243–252. https://doi.org/10.1111/ele.12889

Stewart, I. T., Cayan, D. R., & Dettinger, M. D. (2005). Changes toward earlier streamflow timing across western North America. *Journal of Climate*, *18*(8), 1136–1155. https://doi.org/10.1175/jcli3321.1

Stewart, I. T. (2009). Changes in snowpack and snowmelt runoff for key mountain regions. *Hydrological Processes*, *23*(1), 78–94. https://doi.org/10.1002/hyp.7128

Stinson, K. A. (2005). Effects of Snowmelt Timing and Neighbor Density on the Altitudinal Distribution of Potentilla diversifolia in Western Colorado, U.S.A. *Arctic, Antarctic, and Alpine Research*, *37*(3), 379–386. https://doi.org/10.1657/1523-0430(2005)037[0379:EOSTAN]2.0.CO;2

Sun, N., Yan, H., Wigmosta, M. S., Lundquist, J., Dickerson-Lange, S., & Zhou, T. (2022). Forest canopy density effects on snowpack across the climate gradients of the Western United States Mountain Ranges. *Water Resources Research*, *58*(1). https://doi.org/10.1029/2020wr029194

Surunis, A., & Gleason, K. E. (2024). Modelling postfire recovery of snow albedo and forest structure to understand drivers of decades of reduced snow water storage and advanced snowmelt timing. *Hydrological Processes*, *38*(7), e15246. https://doi.org/10.1002/hyp.15246

Swayze, N., Choi, C. T. H., Knowlton, G., & Klisauskaite, J. (2021, May 14). *Colorado Front Range Disasters: Understanding the Impact of Forest Management on the Cameron Peak and CalWood Fire*. https://ntrs.nasa.gov/citations/20210014944

Tarricone, J., Palomaki, R., Rittger, K., Nolin, A., Marshall, H.-P., & Vuyovich, C. (2025). Investigating the impact of optical snow cover data on L-band Insar Snow Water equivalent retrievals. *Journal of Remote Sensing*, *5*. https://doi.org/10.34133/remotesensing.0682

Tait, A. B. (1998). Estimation of Snow Water Equivalent Using Passive Microwave Radiation Data. *Remote Sensing of Environment*, *64*(3), 286–291. https://doi.org/10.1016/S0034-4257(98)00005-4

Tanniru, S., & Ramsankaran, R. (2023). Passive Microwave Remote Sensing of Snow Depth: Techniques, Challenges and Future Directions. *Remote Sensing*, *15*(4), Article 4. https://doi.org/10.3390/rs15041052

TC - Sentinel-1 snow depth retrieval at sub-kilometer resolution over the European Alps. (n.d.). Retrieved October 23, 2024, from https://tc.copernicus.org/articles/16/159/2022/

Tedesche, M. E., Trochim, E. D., Fassnacht, S. R., & Wolken, G. J. (2022). Brooks Range Perennial Snowfields: Extent Detection from the Field and via Satellite. *The Cryosphere Discussions*, 1–29. https://doi.org/10.5194/tc-2022-143

Tedesco, M., & Miller, J. (2007). Observations and statistical analysis of combined active–passive microwave space-borne data and snow depth at large spatial scales. *Remote Sensing of Environment*, *111*(2), 382–397. https://doi.org/10.1016/j.rse.2007.04.019

The Sentinel missions. (n.d.). Retrieved September 4, 2024, from https://www.esa.int/Applications/Observing_the_Earth/Copernicus/The_Sentinel_missions

Time-series snowmelt detection over the Antarctic using Sentinel-1 SAR images on Google Earth Engine—ScienceDirect. (n.d.). Retrieved September 16, 2024, from https://www.sciencedirect.com/science/article/pii/S0034425721000365

Trevisiol, F., Mandanici, E., Pagliarani, A., & Bitelli, G. (2024). Evaluation of Landsat-9 interoperability with Sentinel-2 and Landsat-8 over Europe and local comparison with field surveys. *ISPRS Journal of Photogrammetry and Remote Sensing*, *210*, 55–68. https://doi.org/10.1016/j.isprsjprs.2024.02.021

Trujillo, E., & Molotch, N. P. (2014). Snowpack regimes of the Western United States. *Water Resources Research*, *50*(7), 5611–5623. https://doi.org/10.1002/2013WR014753

Tsai, Y.-L. S., Dietz, A., Oppelt, N., & Kuenzer, C. (2019). Wet and Dry Snow Detection Using Sentinel-1 SAR Data for Mountainous Areas with a Machine Learning Technique. *Remote Sensing*, *11*(8), Article 8. https://doi.org/10.3390/rs11080895

Turner, M. G., Braziunas, K. H., Hansen, W. D., & Harvey, B. J. (2019). Short-interval severe fire erodes the resilience of subalpine lodgepole pine forests. *Proceedings of the National Academy of Sciences*, *116*(23), 11319–11328. https://doi.org/10.1073/pnas.1902841116

Vanderhoof, M. K., Alexander, L., Christensen, J., Solvik, K., Nieuwlandt, P., & Sagehorn, M. (2023). High-frequency time series comparison of Sentinel-1 and Sentinel-2 satellites for mapping open and vegetated water across the United States (2017–2021). *Remote Sensing of Environment*, *288*, 113498. https://doi.org/10.1016/j.rse.2023.113498

Varade, D., Manickam, S., Dikshit, O., Singh, G., & Snehmani. (2020). Modelling of early winter snow density using fully polarimetric C-band SAR data in the Indian Himalayas. *Remote Sensing of Environment*, *240*, 111699. https://doi.org/10.1016/j.rse.2020.111699

Veblen, T. T., Kitzberger, T., & Donnegan, J. (2000). Climatic and human influences on fire regimes in ponderosa pine forests in the Colorado Front Range. *Ecological Applications*, *10*(4), 1178. https://doi.org/10.2307/2641025

Vollrath, A., Mullissa, A., & Reiche, J. (2020). Angular-Based Radiometric Slope Correction for Sentinel-1 on Google Earth Engine. *Remote Sensing*, *12*(11), Article 11. https://doi.org/10.3390/rs12111867

Walker, A. E., & Goodison, B. E. (1993). Discrimination of a wet snow cover using passive microwave satellite data. *Annals of Glaciology*, *17*, 307–311. https://doi.org/10.3189/S026030550001301X

Wang, Y., Su, J., Zhai, X., Meng, F., & Liu, C. (2022). Snow Coverage Mapping by Learning from Sentinel-2 Satellite Multispectral Images via Machine Learning Algorithms. *Remote Sensing*, *14*(3), Article 3. https://doi.org/10.3390/rs14030782

Wang, Z., Erb, A. M., Schaaf, C. B., Sun, Q., Liu, Y., Yang, Y., Shuai, Y., Casey, K. A., & Román, M. O. (2016). Early spring post-fire snow albedo dynamics in high latitude boreal forests using Landsat-8 OLI data. *Remote Sensing of Environment*, *185*, 71–83. https://doi.org/10.1016/j.rse.2016.02.059

Water | Free Full-Text | Assessing Watershed-Wildfire Risks on National Forest System Lands in the Rocky Mountain Region of the United States. (n.d.). Retrieved October 19, 2023, from https://www.mdpi.com/2073-4441/5/3/945

Warziniack, T., & Brown, T. C. (2019). The importance of municipal and agricultural demands in future water shortages in the United States. *Environmental Research Letters*, *14*(8), 084036. https://doi.org/10.1088/1748-9326/ab2b76

Wasserman, T. N., & Mueller, S. E. (2023). Climate influences on future fire severity: A synthesis of climate-fire interactions and impacts on fire regimes, high-severity fire, and forests in the Western United States. *Fire Ecology*, *19*(1). https://doi.org/10.1186/s42408-023-00200-8

Wendleder, A., Dietz, A. J., & Schork, K. (2018). Mapping Snow Cover Extent Using Optical and SAR Data. *IGARSS 2018 - 2018 IEEE International Geoscience and Remote Sensing Symposium*, 5104–5107. https://doi.org/10.1109/IGARSS.2018.8518374

Westerling, A. L., Hidalgo, H. G., Cayan, D. R., & Swetnam, T. W. (2006). Warming and Earlier Spring Increase Western U.S. Forest Wildfire Activity. *Science*, *313*(5789), 940–943. https://doi.org/10.1126/science.1128834

Williams, C. H. S., Silins, U., Spencer, S. A., Wagner, M. J., Stone, M., & Emelko, M. B. (2019). Net precipitation in burned and unburned subalpine forest stands after wildfire in the northern Rocky Mountains. *International Journal of Wildland Fire*, *28*(10), 750–760. https://doi.org/10.1071/WF18181

Williams, M. A., & Baker, W. L. (2012). Comparison of the Higher-Severity Fire Regime in Historical (A.D. 1800s) and Modern (A.D. 1984–2009) Montane Forests Across 624,156 ha of the Colorado Front Range. *Ecosystems*, *15*(5), 832–847. https://doi.org/10.1007/s10021-012-9549-8

Wulder, M. A., Roy, D. P., Radeloff, V. C., Loveland, T. R., Anderson, M. C., Johnson, D. M., Healey, S., Zhu, Z., Scambos, T. A., Pahlevan, N., Hansen, M., Gorelick, N., Crawford, C. J., Masek, J. G., Hermosilla, T., White, J. C., Belward, A. S., Schaaf, C., Woodcock, C. E., … Cook, B. D. (2022). Fifty years of Landsat science and impacts. *Remote Sensing of Environment*, *280*, 113195. https://doi.org/10.1016/j.rse.2022.113195

Xu, H., Chen, J., He, G., Lin, Z., Bai, Y., Ren, M., Zhang, H., Yin, H., & Liu, F. (2024). Immediate assessment of forest fire using a novel vegetation index and Machine Learning based on multi-platform, high temporal resolution remote sensing images. *International Journal of Applied Earth Observation and Geoinformation*, *134*, 104210. https://doi.org/10.1016/j.jag.2024.104210

Zhou, C., & Zheng, L. (2017). Mapping Radar Glacier Zones and Dry Snow Line in the Antarctic Peninsula Using Sentinel-1 Images. *Remote Sensing*, *9*(11), Article 11. https://doi.org/10.3390/rs9111171

Zhu, J., Tan, S., Tsang, L., Kang, D.-H., & Kim, E. (2021). Snow Water Equivalent Retrieval Using Active and Passive Microwave Observations. *Water Resources Research*, *57*(7), e2020WR027563. https://doi.org/10.1029/2020WR027563

Zschenderlein, L., Luojus, K., Takala, M., Venäläinen, P., & Pulliainen, J. (2023). Evaluation of passive microwave dry snow detection algorithms and application to SWE retrieval during seasonal snow accumulation. *Remote Sensing of Environment*, *288*, 113476. https://doi.org/10.1016/j.rse.2023.113476